6
Nano A-M

Encyclopedia of

NANOSCIENCE and NANOTECHNOLOGY®

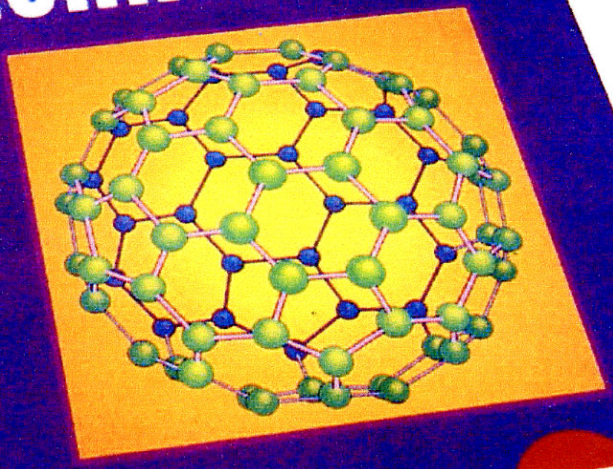

Edited by
Hari Singh Nalwa

Foreword by
Richard E. Smalley, Nobel Prize Laureate

ASP
AMERICAN SCIENTIFIC PUBLISHERS

ENN Encyclopedia of Nanoscience and Nanotechnology
www.aspbs.com/enn

Nanohelical/Spiral Materials

S. Motojima, X. Chen

Gifu University, Gifu 501-1193, Japan

CONTENTS

1. INTRODUCTION

In cosmos and in nature, maelstrom, spiral, helical, or coil structures, such as a whirled air (typhoons), whirled seawater, vine plants, shellfish, proteins, DNA, etc. are commonly observed. The helical/spiral shapes are also commonly observed in artificial water screws, spiral staircases, retaining screws, bolts/nuts, screw dislocations in solids, etc. Furthermore, electromagnetic waves, spirit or mind, economic cycles, etc. have also a helical/spiral motion pattern. That is, three-dimensional (3D)-helical/spiral structures are the fundamental structure of many natural objects, including science and human livings. The helical morphology of DNA or proteins has essential and critical functional roles in living bodies. Recently, the double helix-shaped DNA, single-helix-shaped proteins, or chiral carbon nanotubes have been attracting attention in biotechnology and nanotechnology [1–3]. Materials with 3D-helical/spiral structures with micrometer to nanometer order dimensions have not been commercially available. Motojima and Chen have prepared regularly coiled carbon fibers (carbon coils) with 3D-helical/spiral structures, which are similar structures to all things in the cosmos, with high coil yield. We named them "cosmomimetic carbon coils" for these carbon coils after "biomemetics" [1]. The helical/spiral materials are expected to have novel functionality and many potential applications such as tunable microdevices/sensors, electromagnetic absorbers, energy changing materials, hydrogen absorbers, chiral catalysts, activators of organisms, etc. In addition to their potential applications, the growth mechanism is very interesting from the scientific point of view.

Although some helical/spiral-formed fibers are referred to in comprehensive reviews on the vapor grown carbon fibers, by Rodriguez [4] and de Jong and Geus [5], up to now, there has not been any comprehensive review on nanohelical/spiral materials.

In this chapter, we will introduce the preparation processes, morphologies, microstructures, and properties of the helical/spiral-structured substances such as carbon nanocoils and ceramic nanocoils/nanotubes. We also discuss the growth mechanism of the helical/spiral structure and predict the possible applications.

2. CARBON NANOCOILS

2.1. Introduction

In 1953, Davis and co-workers [6, 7] were the first to report the vapor growth of thin carbon fibers twisted together in the form of a rope. The observation of helical/spiral-coiled carbon nanofibers, with a coil diameter of several micrometers to several nanometers (referred to as "carbon nanocoils" hereafter), from vapor phase using a chemical vapor deposition (CVD) process, were then reported by some carbon filament researchers. Since from the 1970s to the 1980s, Baker and co-workers reported the observation of carbon twisted fibers among the Fe-group metal-catalyzed vapor grown carbon filaments. Furthermore, they extensively studied the effects of H_2, Cu, Pt, Sn, and other oxides on the growth of carbon filaments and observed the growth of helical carbon filaments. However, before 1990, carbon coils grown by the CVD process were extremely accidental, reproducibility was very poor, and the production was almost excluded as anomalous and unpreferable deposits with helical/spiral forms.

In 1990, Motojima and co-workers [8] first found that regular-coiled carbon fibers (carbon nanocoils) could be obtained with high reproducibility by the catalytic pyrolysis of acetylene containing a small amount of sulfur impurities over transition metal catalysts, and then they extensively examined the preparation conditions, morphology, growth mechanisms, and some properties in detail. Meanwhile, Motojima and co-workers [9–11] also first found that very regularly coiled silicon nitride (Si_3N_4) fibers could be obtained by the CVD process. After then, various ceramic coils such as metal carbides, nitrides, and oxides were prepared by the CVD, sol/gel, diffusion, template processes, etc.

ISBN: 1-58883-062-4/$35.00

Encyclopedia of Nanoscience and Nanotechnology
Edited by H. S. Nalwa
Volume 6: Pages (775–794)

Since 2000, carbon coils have attracted interest and carbon coils with diverse morphologies have been reported by many researchers. Among various preparation processes, the CVD process is the process with the most potential for the large-scale preparation of pure carbon coils. So the preparation of carbon coils has been mainly carried out using various CVD reaction systems, mainly using Fe-group metal catalysts and acetylene or ethylene carbon sources.

In this section, we will first summarize some of the earlier literature in which the growth of helical-coiled carbon fibers is referred. Thereafter, we will present recent research progress in the preparation (processes and conditions), morphology, microstructure, and some properties, and we will discuss the growth mechanism. Finally we will predict the potential applications of the carbon nanocoils.

2.2. Preparation, Morphology, and Microstructure

In 1953, Davis and co-workers [6, 7] first reported the vapor growth of thin carbon fibers twisted together in the form of a rope (helical threads) by the disproportionation of CO over iron compound catalysts at 450 °C. The obtained helical threads are apparently hollow and are probably formed by coiling of flat ribbons. In 1958, Hillert and Lange [12] reported the growth of a single helical thread and combinations of three helical thread, parallel, or twisted forms from N_2-heptane source gas mixtures at 1000 °C using Fe catalyst. In 1972, Baker and co-workers [13] reported the growth of twisted carbon fibers with a coil diameter of about 60 nm from a C_2H_2/H_2 (or O_2) gas mixture at 870–1100 K using the Ni catalyst. They introduced H_2 or O_2 to the reaction system preventing Ni particles from being deactivated and found that the catalytic activity of the Ni particles for filament growth ceased after approximately 15 s at 870 K, but it could be regenerated by exposure to H_2 at 1100 K or O_2 at 1000 K. Boehm [14] also obtained carbon braided fibers with herringbone structure by the disproportionation of CO at 650 °C over $Fe(CO)_5$ or $Ni(CO)_4$ catalyst. He proposed a growth model for the helical fiber formation, in which he suggested that iron carbide formed on the disorganized carbon, and braided fibers formed on the crystal faces of iron carbide.

In recent years, Park and Baker [15, 16] paid much attention to the growth of carbon filaments by decomposition of ethylene over Fe-group alloy catalysts. During their investigation of the decomposition of a $C_2H_4/CO/H_2$ gas mixture over a series of Fe/Ni catalysts, and detailed analysis of both the gaseous products and the amount of the deposited solid carbons, they revealed that co-adsorption of the two carbon-containing gases produced major modifications in the behavior of the bimetallic catalyst surfaces. It was evident that the addition of CO to a C_2H_4/H_2 gas mixture resulted in a substantial increase in the decomposition of the olefin over all the bimetallic catalyst powders with this effect being most pronounced on the Fe-rich systems. The major product from this series of Fe/Ni catalysts was found to be solid carbon in the form of various filamentous structures, including twisted carbon nanocoils with 200 nm diameter produced from the interaction of an Fe catalyst with a $C_2H_4/CO/H_2$(3:1:1) gas mixture at a 600 °C. A growth tip with bidirectional mode can be seen, as can the tightly coiled nature of filaments grown with 200 nm diameter from the interaction of an Fe–Ni(2:8) catalyst with a $C_2H_4/CO/H_2$(3:1:1) gas mixture at 600 °C.

Great attention has been paid to the effect of the impurity on the catalytic effect of Fe-group metals. Baker and co-workers [17] studied the influence of Sn on Fe catalyst and obtained spiral carbon filaments from acetylene at above 800 °C by using the Sn/Fe (Sn coated Fe foils) catalyst. The filaments were nearly all spiraling with a constant coil pitch and commonly branched. Two spiral filaments generally grew from a catalyst particle in opposite directions. Branching of filaments was frequently observed. They found that the addition of Sn into Fe can prevent the catalyst from being poisoned. Baker and Waite [18] also studied the preparation of carbon filaments by the Pt/Fe alloy-catalyzed pyrolysis of C_2H_2 and found that using this alloy at 690 K, which is a much lower temperature than that using pure Fe, carbon filament grew two orders of magnitude faster than pure Fe. But at a higher temperature, 1175 K, and using ethylene as a carbon source, the growth of very short coils was observed.

In 1984, Galuszka and Back [19] studied the catalytic activity of Fe films formed by thermal decomposition of a solution of ferric nitrate in the presence of mercury vapor. They found that this iron catalyst induced the formation of filamentous carbon during the pyrolysis of methane and that oxidation–reduction of the sputtered iron was shown to lead to fragmentation of the films into particles with a size suitable for the growth of filaments. Among the deposits the springlike single-helix carbon nanofibers were observed.

In 1992, Kim and co-workers [20] used a Cu/Ni (1:1) as the catalyst and acetylene as the carbon source for obtaining the carbon fibers and found that two filaments grew from opposite faces of the catalyst particle at identical rates. Furthermore, during the major part of the growth process, the filaments were relatively smooth and tended to form into large loops. Over a period of time it became clear that many of the filaments were slowly decreasing in width, as a result of catalyst material being dissipated within the structure, and this behavior frequently resulted in the creation of secondary smaller filaments on the parent growth. Furthermore, they also suggested that when the particles reached a size of about a third of the original value, the filaments appeared to undergo a further change in shape and simultaneously started to rotate on an axis perpendicular to the direction of filament growth, causing the filament to acquire a spiral form. When the catalyst is Ni-rich, Cu/Ni (1:1), supported on graphite, 2 Torr, C_2H_2, bidirectional filaments with a spiraling mode grew. But when Cu-rich, Cu/Ni (7:3) + C_2H_4/H_2(1:4) at 600 °C, Cu-rich particles tend to grow in a spiral conformation.

Furthermore, in 1997, Krishnankutty and co-workers [21] continued to report the effect of Cu on the structural characteristics of the carbon filaments produced from Fe-catalyzed decomposition of ethylene. Carbon filaments were produced by the decomposition of ethylene over unsupported Fe/Cu catalyst powders in the presence of varying amounts of H_2 at 500–800 °C. Helical coils could be obtained using a Fe/Cu (3:7) catalyst and C_2H_4/H_2 (1:4) at 500–600 °C. With catalysts rich in Cu, it was apparent

that although the resulting carbon filaments continued to grown via bidirectional mode, there was a subtle difference in that they acquired a helical conformation. The herringbone arrangement of the graphite platelets is indicated in the catalyst grain present on the fiber tip. Two structures, herringbone (platelets oriented at an angle with respect to the fiber axis with smooth surfaces) and tubular arrangements models, are presented. The effects of Cu in Ni catalysts have been also reported by Bernado and co-workers [22, 23] and Jong and co-workers [24] recently.

Hernadi and co-workers [25] reported the growth of carbon coils in preparation of carbon nanotubes from acetylene at 700 °C over Fe/silica supported catalyst. The carbon coil is a single-helix coil and has a coil diameter of about 80 nm and a coil pitch of about 160 nm as shown in Figure 1. Grobert and co-workers [26] obtained carbon nanocoils by the pyrolysis of solid organic precursor (for example, 2-amino-4, 6-dichloro-*s*-triazine, *s*-triamono-triazine) at 950–1050 °C using laser patterned thin metal (Fe, Co, Ni) as the catalyst and silica substrate. The obtained nanocoils have a coil diameter of 1.2–0.6 μm and a coil pitch of 3-0.3 μm as shown in Figure 2a. Simulated single-walled corkscrew-like carbon nanotubes produced by interspersing five- and seven-membered rings judiciously within the mainly hexagonal network is also depicted in Figure 2b.

Recently, Chesnokov and co-workers [27] reported the growth regularities and mechanism of symmetric twisted carbon filaments formed from butadiene-1, 3 on Ni–Cu/MgO-catalyst at 450 °C. Dissymetrical spirally twisted carbon filaments have been shown to grow from a single Ni/Cu alloy particle. They suggested that as the filaments grow, a microphase of metastable nickel carbide (Ni_3C) forms on the particle's frontal side, whereas the crystal particle of Ni/Cu alloy possesses a series of twinning planes (111) that are parallel to the dissymmetry plane of the crystal and separate the blocks of twins from a face-centered structure.

Although it is well known that sulfur acts as a poison for many Ni catalyzed reactions, it is now being recognized that certain benefits can be derived from following a partial and well controlled sulfidation treatment of the metal. Owens and co-workers [28] reported the effect of sulfur on the interaction of Ni with ethylene. They found the enhancement in carbon filament growth following pretreatment of Ni in low levels of H_2S (4–50 ppm) is related to a reconstruction of the metal surface. The inhibition of catalytic activity resulting from a more severe pretreatment in H_2S is ascribed to the formation of a 2D or 3D bulk sulfide. They considered that re-adsorption of S on Ni induced some major perturbations in the morphological characteristics of the filamentous carbon deposits, which are generated in the form of regularly coiled structures. In contrast, those produced from unadulterated metal particles were found to be relatively straight. This change in growth mode indicates that sulfur is modifying the diffusion characteristics of carbon species through the catalyst particle.

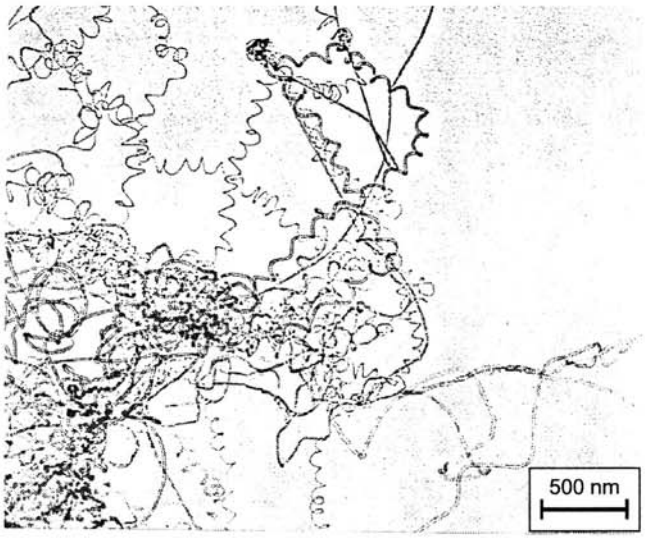

Figure 1. Carbon nanotubes formed in the decomposition of acetylene at 700 °C over Fe/silica (ion-adsorption precipitation using pH = 9 as initial solution, but the pH was close to 7 before filtration) catalyst.

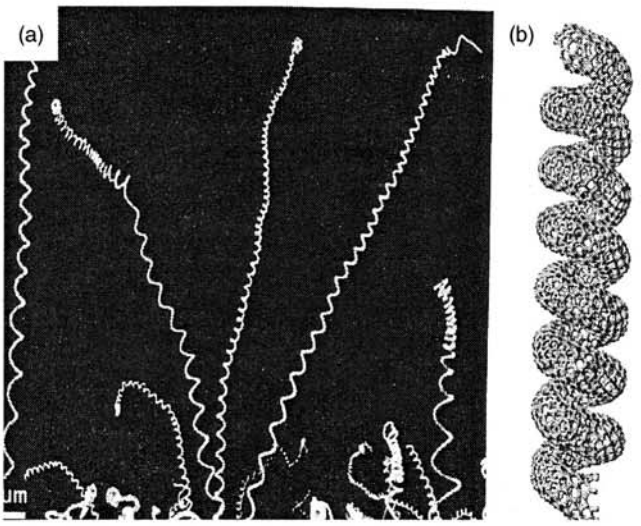

Figure 2. (a) Scanning electron microscope image of carbon nanocoils generated by pyrolysis of melamine over Co "aged" catalyst substrate (in air). (b) Simulated single-walled corkscrew-shaped carbon nanotube produced by interspersing five- and seven-membered rings judiciously within the mainly hexagonal network [26].

Motojima and co-workers [8] first found that the regularly coiled carbon coils could be obtained with high reproducibility by the catalytic pyrolysis of acetylene, containing a small amount of S impurity, and then extensively examined the relationship between coil yield and preparation conditions, as well as morphology, growth mechanism, and some properties in detail. This process makes it possible to prepare carbon coils in semimass while, to our knowledge, the coil yield of carbon nanocoils is rarely reported by other research group so far. These results are comprehensively presented in the following section.

Figueiredo and co-workers [29] obtained carbon nanocoils by Co-catalyzed pyrolysis of acetylene. The obtained nanocoils are single-helix coils and have very small coil diameters of about 60 nm as can be seen in Figure 3. Rodoriguez and co-workers [30] prepared carbon filaments by pyrolysis of ethane containing a H_2S at 815 to 865 °C using Fe/Ni catalyst. It was observed that a dramatic change occurred in catalyst activity and selectivity when 50 ppm H_2S was added

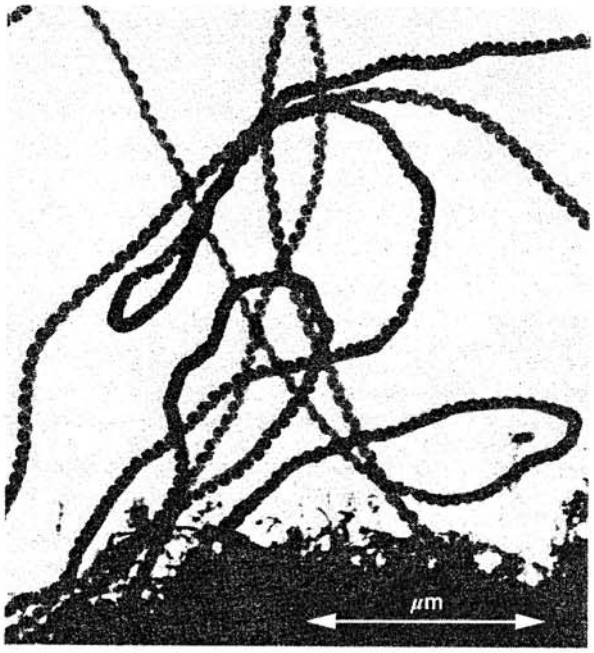

Figure 3. Helical filaments formed during the reaction of cobalt with acetylene [29].

to the ethane feed. Graphite shell-like deposits were predominant in the case of the Fe/Ni (5:5) catalyst, while carbon nanofibers in the case of the Fe/Ni (8:2) catalyst were predominant. Carbon nanocoils with a coil diameter of about 700 nm and a coil pitch of about 400 nm were obtained by the pyrolysis of ethane at 815 °C using the Fe/Ni(8:2) catalyst.

Amelinckx and co-workers [31] prepared helix-shaped carbon tubules by the Co-catalyzed pyrolysis of acetylene and examined in detail the morphology and microstructure. The different morphologies and transmission electron microscopy (TEM) images of a tubule are shown in Figures 4 and 5, respectively. Figure 4a shows the helix-shaped tubules having pitches of different magnitudes. Figure 4b shows the complicated interaction between straight and helix-shaped tubules. Figure 4c shows the parallel arrangement of a straight and a helix-shaped tubule, presumably kept together by van der Waals attraction. Figure 4d shows the coiled tubule intercoiling with itself after having made a U-turn. Figure 4e shows the straight tubules making

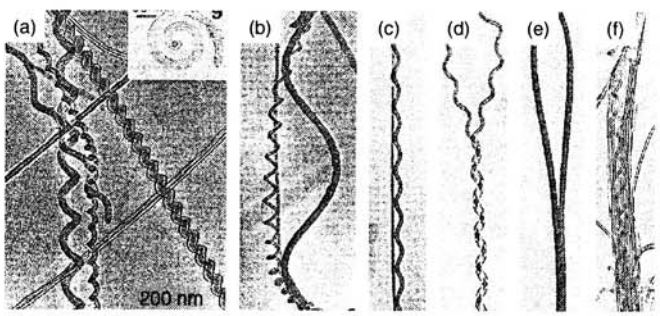

Figure 4. Graphite tubules grown by the Co-catalyzed decomposition of acetylene, exhibiting various shapes [31].

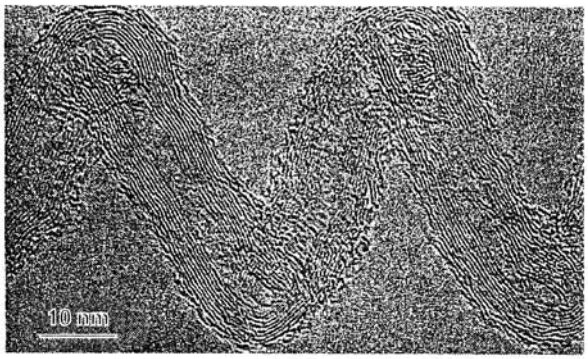

Figure 5. High-resolution images of a helix-shaped tubule containing 11 graphene tubules as shown Figure 4a [31].

a closed loop, the straight ends sticking together. Figure 4f shows the bundle of parallel straight tubules and one helix. Figure 4g shows the planar spiral-shaped tubule. It can be seen that these tubules are a multiwalled nanotube. They also introduced the concept of a spatial-velocity hodograph to explain the growth mechanism of the helix-shaped carbon tubules as shown in Section 2.6.

Krishnankutty and co-workers [21] reported the effect of Cu addition on the decomposition of C_2H_4 in H_2 over Fe catalyst at 450–800 °C. The addition of only 2 wt% Cu to Fe caused a 20-fold increase in the amount of carbon filaments formed compared to that produced on pure Fe at 600 °C. They suggested that this behavior is probably caused by inducing electronic perturbations in the Fe atoms, which results in a modification in the chemisorption characteristics of C_2H_2 on such a surface. Carbon coils with a coil diameter of 1.5 μm were obtained by the Fe/Cu (3:7)-catalyzed pyrolysis of ethylene at 500–600 °C as shown in Figure 6. The TEM image showed that there are two structures: a herringbone structure in which platelets are oriented at an angle with respect to the fiber axis as shown in Figure 7a and a tubular structure in Figure 7b. These structures are very indicative of the carbon coils as well as carbon nanotubes.

Mao and Xie [32] reported that carbon nanotubes with a coil diameter below 100 nm could be obtained from acetylene (10% in N_2) at 650 °C in 150 Torr using a Co-implanted

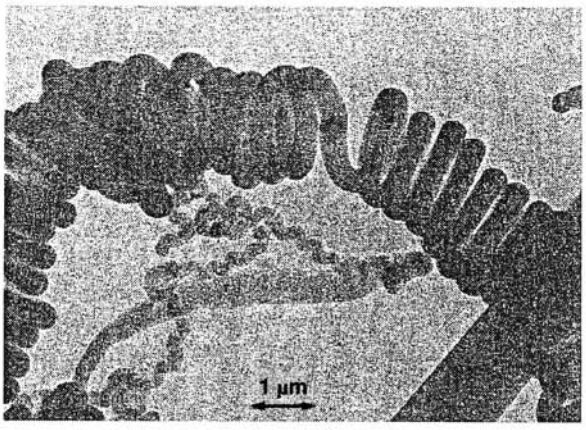

Figure 6. Transmission electron micrograph showing the appearance of carbon filaments produced from the Fe/Cu (3:7) catalyzed decomposition of an ethylene/hydrogen (1:4) mixture at 600 °C [21].

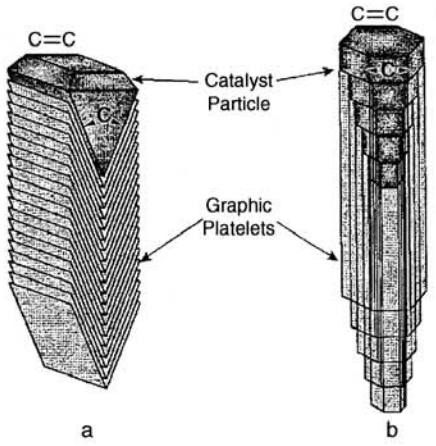

Figure 7. Schematic diagram highlighting the essential steps involved in the catalytic growth of carbon filaments from decomposition of a hydrocarbon and the alignment of graphite platelets in the filament structures: (a) herringbone and (b) tubular arrangements [21].

Ge substrate (Co dose: 1×10^{17} cm^2). The formation of these helical nanotubes is considered to be attributed to the different growth velocities of the tubes from different facets of the nanoparticle catalysts as proposed by Amelinckx et al. [31].

Cesar and co-workers [34] reported the synthesis and characterization of twisted carbon filaments with a coil diameter of less than 80 nm by the catalytic pyrolysis of propane using the Pd_3P colloid catalyst at 600 °C. The structure of the filament was amorphous.

Zhang and co-workers [35] prepared carbon tubule nanocoils by the catalytic pyrolysis of propane using Fe-coated indium-tin-oxide (ITO)/glass substrate as the catalyst at 700 °C. The nanocoils usually consist of two or more tubules and each of them grows with its own diameter and pitch. The tubules mostly consist of graphene sheets, and most of the coils have an external diameter range from several tens to several hundred nanometers, most of them are several hundred nanometers. But when using Fe/InO_x or Fe/ SnO_x as the catalysts, the coil yield was very low. It is considered that Fe plays an important role in the growth of the carbon tubes, while In, Sn, O, and/or their alloys contribute to the formation of the coils.

Pan and co-workers [36] reported the synthesis of carbon nanocoils by the electroplated Fe/ITO substrate catalyzed pyrolysis of acetylene at 650–800 °C. The fine Fe particles can be effectively mixed with the ITO in this method, which caused the highly efficient growth of small-sized carbon nanocoils with a 100 nm coil diameter. Pan and co-workers [37] also discussed the effects of Fe and indium in the ITO on the growth of carbon tubule nanocoils. It is found that Fe additions lead to the growth of carbon nanotubes, while ITO induces their helical growth. The yield of carbon nanocoils is determined by the elemental ratio of Sn and In, and high yield is obtained at $Sn/(Sn + In) = 0.1$–0.35.

Lee and co-workers [38] reported the growth of carbon nanofibers by the pyrolysis of acetylene using a Ni-deposited sodalime glass as the catalyst at 500 °C. The diameters of carbon nanofibers are uniformly distributed in the range between 50 and 60 nm. Most of the carbon nanofibers are curved or bent in shape, but some are twisted. They consisted of defective graphitic sheets with a herringbone structure.

Wang and co-workers [39] reported the growth of helical-shaped filaments with a coil diameter of 50–100 nm from a gas mixture of C_6H_6–H_2–Ar at below 520 °C using Fe(or Co, Ni)/γ-Al_2O_3 catalysts by microwave plasma-enhanced CVD. Xie and co-workers [40] also reported the growth of the carbon coils with coil diameters of 5–6 μm by the Ni catalytic pyrolysis of acetylene at 700 °C by the microwave plasma CVD process. Using the plasma CVD process, the addition of sulfur impurity in the reaction atmospheres is not necessary for obtaining carbon coils.

Hernadi and co-workers [41] reported the growth of carbon nanocoils with coil diameters of about 200 nm by the unsupported SnO-doped Fe_3C catalytic pyrolysis of acetylene. Figure 8 shows the carbon nanocoil with different morphologies obtained by them.

Bai [42] reported the preferential growth of nanotubes/nanofibers and nanocoils with controlled diameters by the catalytic pyrolysis of acetylene at 650 °C. Catalyst nanoparticles of a Fe, Co, and Ni were dispersed on the anodized Al plate substrate (Al_2O_3 thickness deposited on Al plate: a few μm), in which a Fe, Co, and Ni sulfate solution was electrochemically impregnated into the nanopores present in an anodized Al plate to deposit fine metal particle. The gas mixture of C_2H_2, N_2, and H_2 (5%) + Ar(95%) flowed onto a quartz reaction tube at a flow rate of 850 sccm. The concentration of C_2H_2 was about 5%. A carbon nanocoil with a coil diameter of 200 nm coil, a coil pitch of 160 nm, and a fiber diameter of about 160 nm was obtained using very fine catalyst particles in the 5–15 nm pores obtained under ac short time electrochemical metal deposition. Carbon coils with a coil diameter of 1.5 μm, a coil pitch of 250 nm, and a fiber diameter of about 200 nm were obtained by longer metal particle deposition times (1 min). Carbon coils with a coil diameter of 16 μm, a coil pitch of 1μm, and a fiber diameter of about 500 nm were obtained with very thin layers composed of large metal particles under 2 min dc deposition conditions.

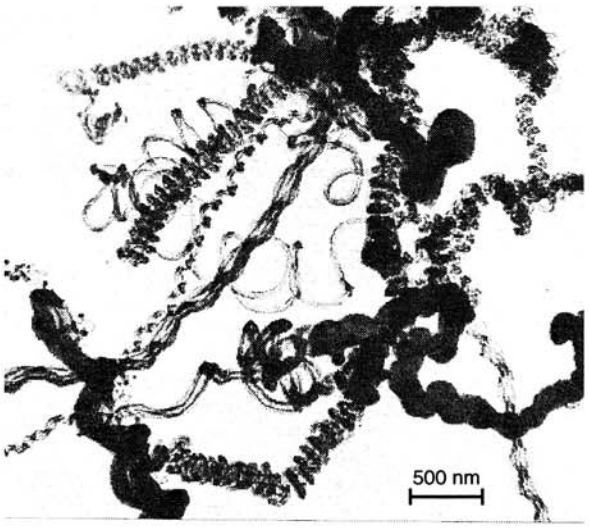

Figure 8. EM image of carbon deposit over $Fe_3C(+SnCl_2)$ [41].

Raman spectroscopy analysis on the carbon coils showed the multiwalled nanotube's nature.

Schliermann and co-workers [43] studied the online-monitoring of gas phase reactions during nanofiber synthesis by fast chromatography. They found that carbon coils grew at the restricted reaction conditions. Hernadi and co-workers [44] prepared the carbon coils with a coil diameter of 100–200 nm and a specific surface area of 44–129 m^2/g from acetylene using the unsupported SnO-doped Fe_3C (direct precipitation) catalyst at 600–800 °C. Jong and co-workers [24] prepared the carbon nanotubes from a CH_4/H_2 gas mixture at $\sim$ 600 °C using the Ni/Cu catalyst by microwave plasma CVD and found that the use of high Cu content catalyst (Cu = 60–80%) results in the growth of helical fibers.

Motojima and co-workers [8, 45–56] examined in detail of the morphology and microstructure of the carbon coils. Figure 9 shows the tip part of the carbon coils obtained using a Ni catalyst [46].

A Ni_3C catalyst grain is always on the tip part of the carbon coils (arrow), and the catalyst grain is the exclusive growth point. Figures 10 and 11 show the enlarged view of the carbon coils [9]. The carbon coils are generally double coils similar to a DNA, and the coil number right-clockwise and left-clockwise is almost the same. Figures 12 and 13 show the carbon coils with interesting morphologies [57]. The growth of a single coil or multiple coils such as shown in Figure 14 was also sometimes observed. Recently, Motojima and co-workers [58, 59] succeeded in preparing carbon nanocoils with a coil diameter of several hundred to several ten nm in large scale using a magnetic CVD process or various catalysts such as Au, Ni/Au, etc. We also studied on the growth of carbon nanocoils by ceramics supported metal catalyzed methods using various metal catalysts such as Fe, Ni, Co, Cu, and supporters such as Al_2O_3, amorphous SiO_2, and molecular sieves. The carbon nanocoils have generally two coiling forms: twisted forms and springlike helix forms such as shown in Figure 15. Using different catalytic systems, many kinds of carbon nanocoils with different morphologies were obtained. Figure 16 shows the tip part of the carbon nanocoils. Two coils [one is right-clockwise coiled and the other is left-clockwise coiled (twisted)] grew from a Ni/Al_2O_3 catalyst grain (arrow). Figure 17 shows the tip part of the carbon coils obtained using the Ni–Fe/molecular sieve catalyst; one coil with fringe on the surface grew from the catalyst grains. The coils in which the chirality and coil axis alternate regularly were prepared by using the Ni–Fe/moleculer sieves or WS_2 catalyst by controlled CVD conditions, and the representative coils are shown in Figures 18 and 19. Double twisted carbon nanofibers as well as 2D zigzag nanofibers were also observed in the Ni/Fe catalyzed deposits (Fig. 20).

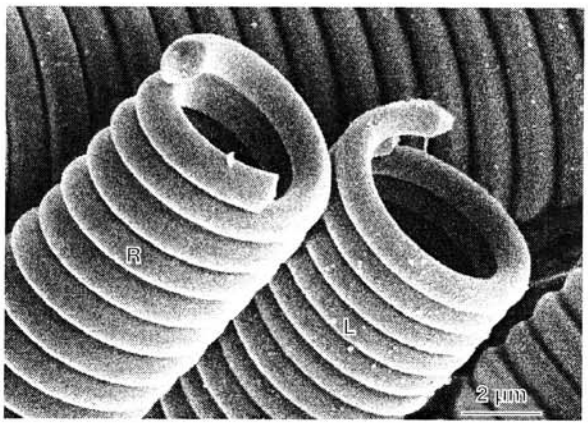

Figure 10. (R) Right-clockwise coiled regular double carbon microcoil. (L) Left-clockwise coiled regular double carbon microcoil. Each has a circular or elliptical fiber cross section [1].

2.3. Large-Scale Preparation of Carbon Nanocoils

In 1990, Motojima and co-workers [8] first found that regularly coiled carbon coils could be obtained with high reproducibility by the catalytic pyrolysis of acetylene containing a small amount of impurities and then extensively examined in detail the preparation conditions, morphology, growth mechanism, and some properties. It was found that the addition of an optimum amount of impurity such as sulfur or phosphorus in the source hydrocarbons is indispensable for obtaining carbon coils with high reproducibility and high coil yield. Between 1993 and 1995, we used phosphorus {PCl_3,

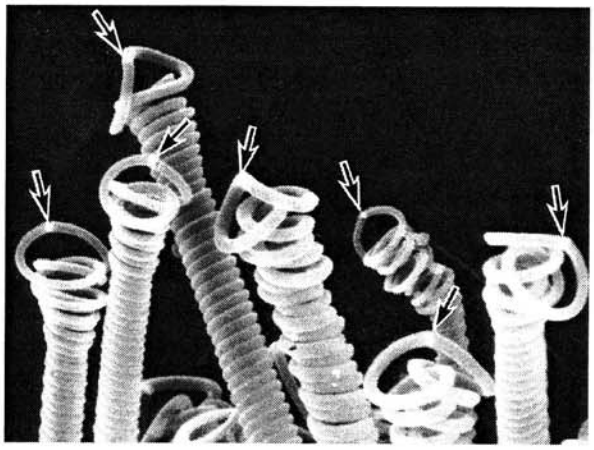

Figure 9. Tip part of the carbon coils obtained using Ni catalyst [1, 46]. Arrow indicates a Ni catalyst grain.

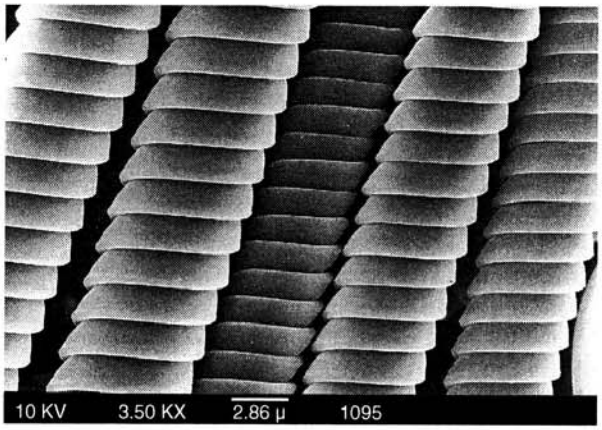

Figure 11. Regular-coiled double carbon microcoils which have a flat or rectangular fiber cross section.

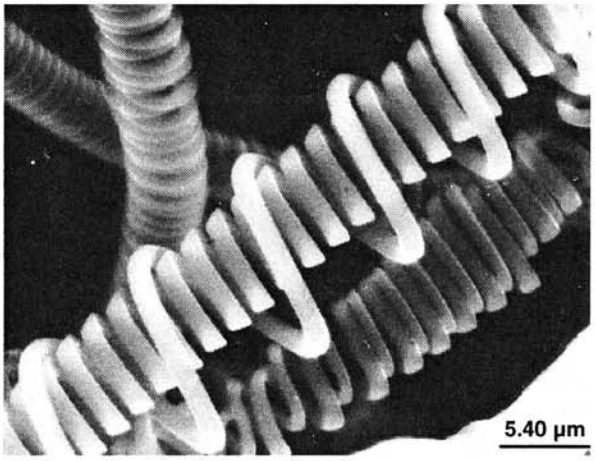

Figure 12. Interesting morphology of the double coils [57].

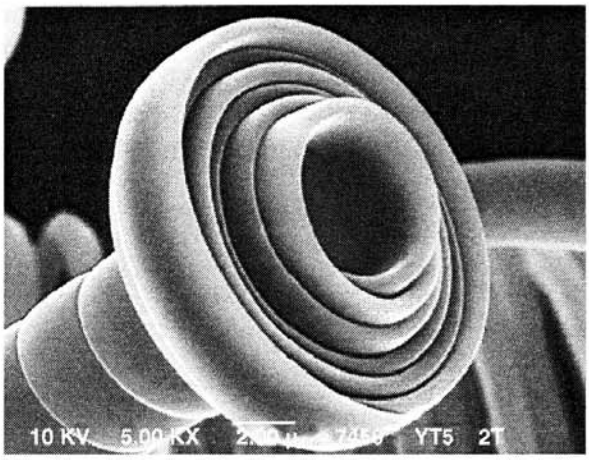

Figure 13. Conically coiled flat carbon coils after growing to the coil axial direction.

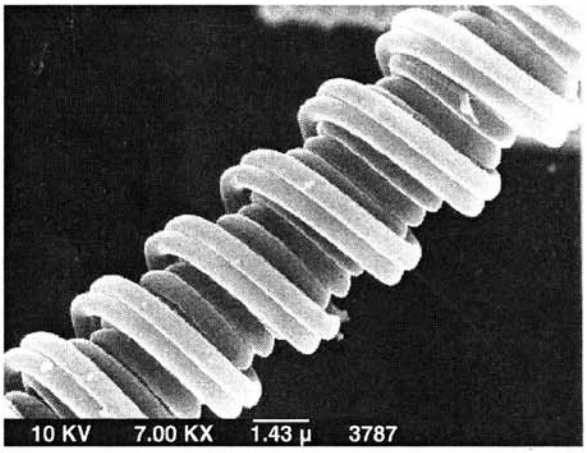

Figure 14. Multiple carbon coils.

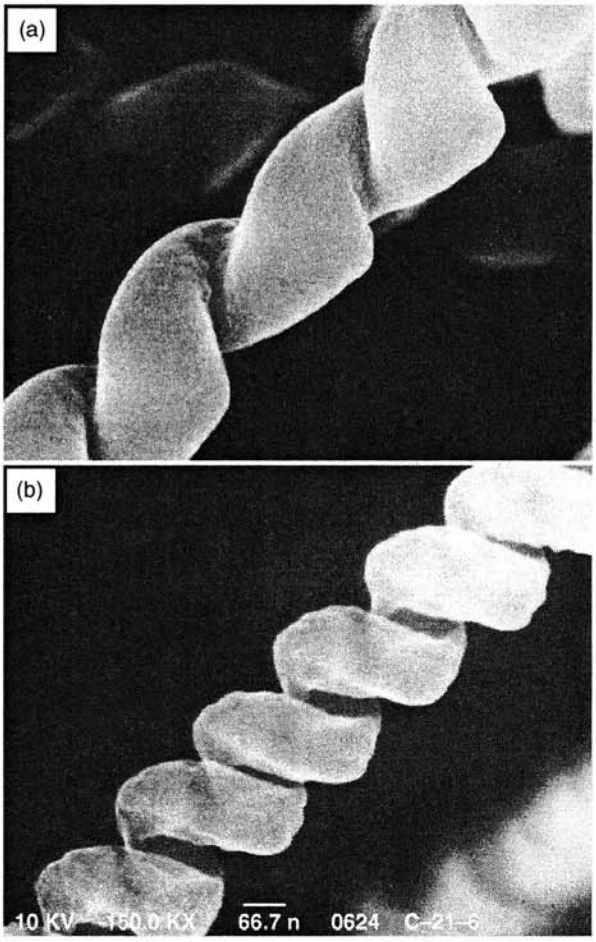

Figure 15. Twisted carbon nanocoils (a) and springlike carbon nanocoils (b).

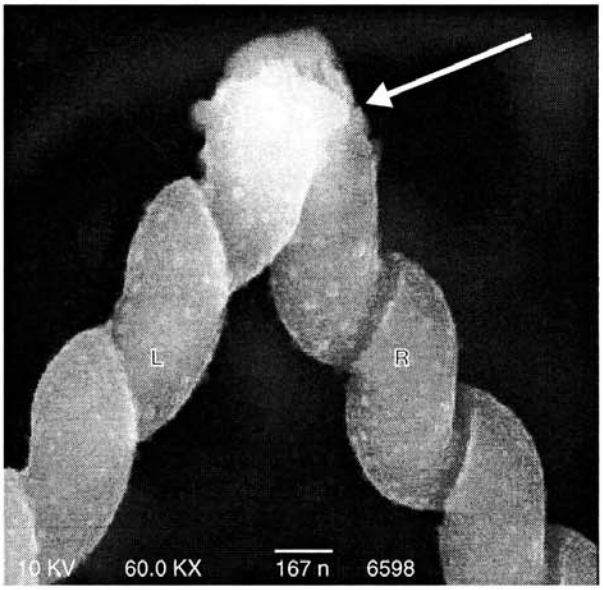

Figure 16. Tip part of the carbon nanocoils. Coiling chirality: (R) Right-clockwise coiling, (L) left-clockwise coiling. Arrow indicates a catalyst grain which is a growing point.

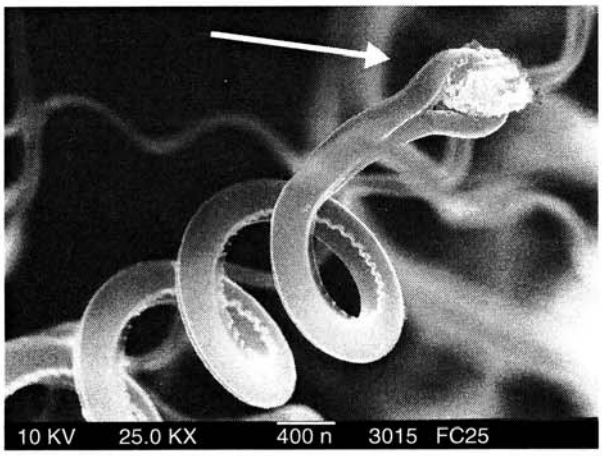

Figure 17. Interesting tip morphology of the carbon coils. Arrow indicates a catalyst grain which is a growing point.

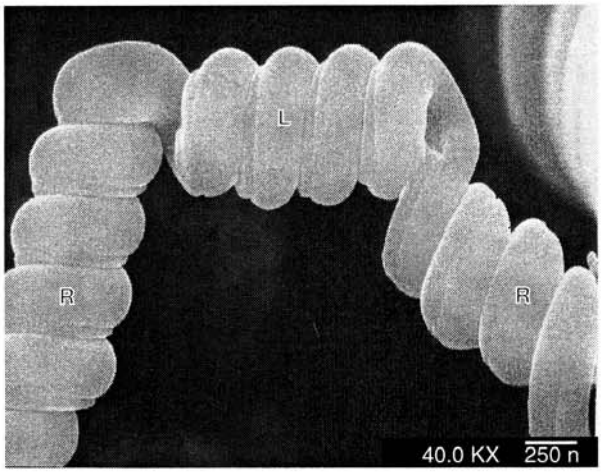

Figure 18. Carbon coils with changed coiling chirality. (R) Right-clockwise coiling, (L) left-clockwise coiling. Catalyst: stainless steel (SUS 304).

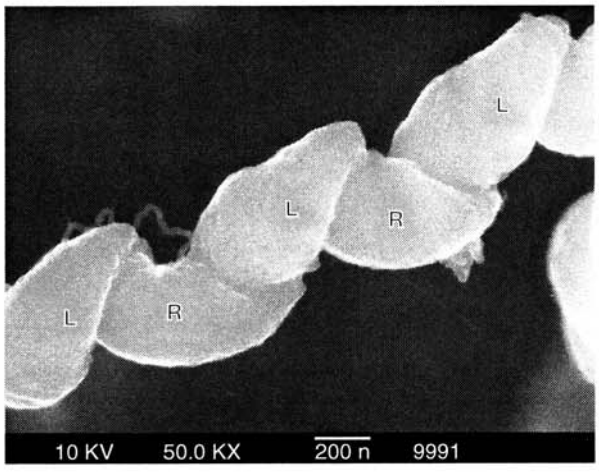

Figure 19. Carbon coils with successively changed coiling chirality. (R) Right-clockwise coiling, (L) left-clockwise coiling. Catalyst: stainless steel (SUS 304).

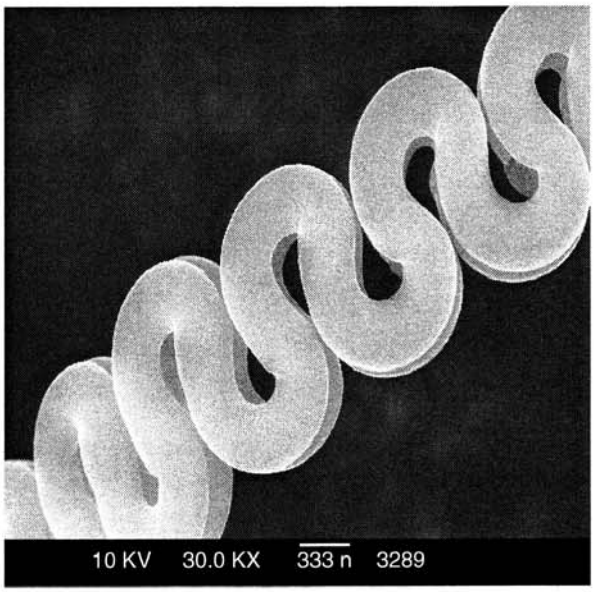

Figure 20. Regular zigzag carbon twin fibers.

PH_3, $(C_2H_5O)_3P$} and sulfur compound impurities (thiophene tetrahydrothiophene, diethylsulfide, hydrogen sulfide, and carbon disulfide) to achieve high yield and good reproducibility, and the maximum coil yield was obtained using a thiophene [60–62]. Since 1995 we have tried to prepare carbon microcoils, using various powders or plates of transition metal carbides such as Co, Cr, Fe, Hf, Mn, Mo, Nb, Ta, Ti, V, and W, Ni single crystal plate, MoS_2, and Ti_2O_3 [62–67]. The results showed that except for Fe, all these metals can be used to obtain carbon coils, but the yield is lower than using a Ni catalyst. Among the carbides used, only TiC powder was effective, but the yield was quite low [63]. MoS_2 and Ti_2O_3 were also effective. Since 1996 [63, 67–73], for producing carbon coils efficiently and economically, extensive efforts were made to improve the reaction device and to optimize the reaction conditions (temperature, gas flow pattern, flow rate of acetylene, thiophene, N_2 and H_2). Multiple gas inlet reactors [72] were developed for the mass-production of the carbon coils. Using this reactor, a coil yield of 0.2 kg/m^2-substrate could be obtained.

2.4. Preparation Process

The carbon coils are usually prepared by a conventional CVD process. Other preparation processes than the conventional CVD are reported as follows.

2.4.1. Laser CVD

Hishikawa and co-workers [74] prepared carbon coils with a coil diameter of 3 μm by the laser CVD process using CO_2 laser from allene (C_3H_4) + sulfur hexafluoride (SF_6) gas mixtures using the Fe catalyst.

2.4.2. Hot-Filament CVD

Motojima and co-workers [75] prepared carbon fibrillform nanocoils by Zn- or Ni-coated Cu catalyzed pyrolysis of ethylene at 600 °C using the hot-filament CVD process.

2.4.3. Microwave-Plasma CVD

Xie and co-workers [40] prepared carbon coils with a coil diameter 3.5 μm and a fiber diameter of 200 nm by the Ni catalyzed pyrolysis of acetylene at 700 °C by the microwave-CVD process. The carbon coils are amorphous and specific surface area is 62 m^2/g.

2.4.4. Plasma and Catalyst Technology Process

Motojima and co-workers [61] prepared carbon coils with irregularly coiled form or with very wide coil pitch of 10–30 μm by the Ni-catalyzed pyrolysis hydrocarbons at 770 °C using a novel plasma and catalyst technology reactor. It was found that hydrocarbons such as methane, propane, and ethylene were decomposed under plasma and catalyst atmospheres to form acetylene as the main decomposition product, and then this acetylene was further decomposed to form carbon coils.

2.4.5. Supersonic CVD

Motojima and co-workers [59, 77] prepared carbon coils under the application of ultrasonic waves in the reaction zone and found that the coil yield and density increased with the application of ultrasonic waves, and that the optimum frequency was 23–28 kHz.

2.4.6. Electromagnetic CVD

In the conventional CVD process, an ac electric heater, from which electromagnetic waves (EM) are emitted, is generally used. Furthermore, the carbon coils can significantly absorb EM waves. Accordingly, it can be reasonably expected that the application of EM field as well as bias voltage in the reaction atmosphere may significantly affect the growth of carbon coils. Motojima and co-workers [59, 69, 78–81] first reported on the effect of the EM waves and bias voltage on the growth and properties of the carbon coils. It was found that the coil yield outstandingly increased by applying EM field and bias voltage on the reaction atmosphere.

2.4.7. Rotation CVD

Motojima and co-workers [70] reported the preparation of carbon coils using the rotation substrate CVD process.

2.4.8. Electroplating Process

Bai [42] obtained carbon nanocoils with a coil diameter of 35 nm and a coil pitch of 30 nm by the electrolysis of NaCl at 810 °C, showing that the CVD process is not the only way to get coiled carbon fibers.

2.5. Microstructure [82–85]

X-ray diffraction (XRD) patterns of the as-grown carbon coils are shown in Figure 21 as well as that of an amorphous pitch-based activated carbon fiber. It can be seen that the carbon coil is almost amorphous. Figure 22 shows the Raman spectra of the as-grown carbon coils obtained by a conventional CVD process and by application of high magnetic field in the reaction atmosphere. It can be seen

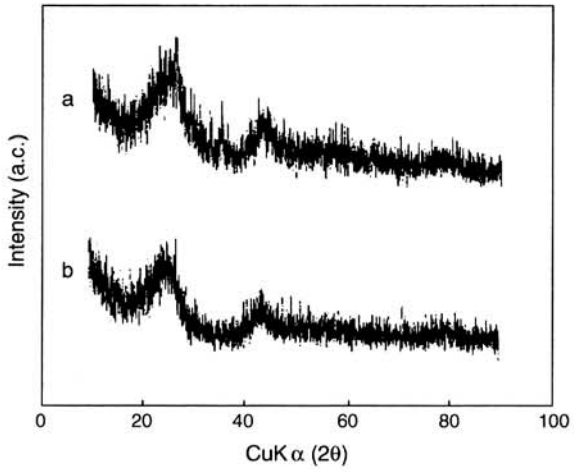

Figure 21. XRD patterns. (a) Pitch-based activated carbon, (b) as grown carbon fibers.

that the D-band and G-band intensity is almost the same, indicating an amorphous state, while the strength of the G-band against the D-band increases with increasing applied magnetic strength. Figure 23 shows the TEM image of the as-grown carbon coils. The development of distinct graphite layers cannot be observed while very short-range orderings can be seen. Figure 24 shows the XRD pattern of the heat treated carbon coils in N_2 or $Co + CO_2$ atmosphere. The amorphous as-grown carbon coils graphitized by the heat treatment without changing coiling morphology, and the graphite coils can be obtained at heat-treatment above 2500 °C. The schematic model of the graphite coils is shown in Figure 25. The graphite coils have distinct graphite layers ($d = 0.339$ nm) with an inclination of 10–40° versus the fiber axis to form a "herringbone" structure.

2.6. Growth Mechanism

Why a vapor grown carbon fiber (VGCF) is sometimes successively curled, twisted, or coiled to form "carbon coils" is very interesting from the theoretical and scientific point of view. In an early stage of the research on the VGCF, the

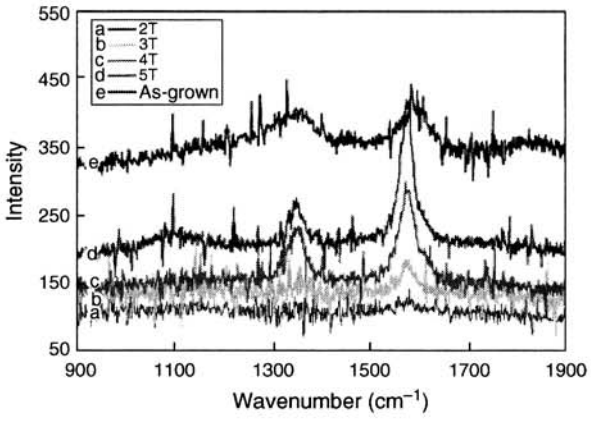

Figure 22. Raman spectra of carbon coils. (a–d): Carbon coils prepared with application of high magnetic field of 2–5 Tesla. (e) As-grown carbon coils.

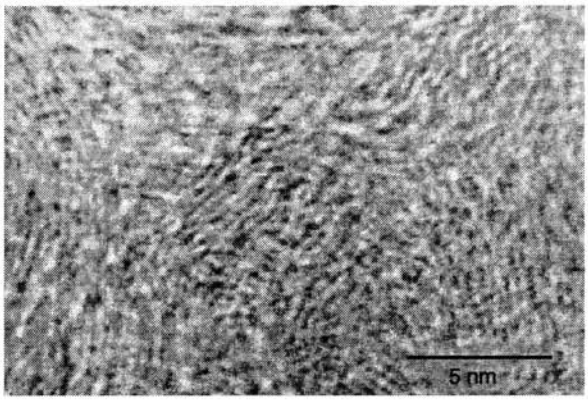

Figure 23. TEM image of the as-grown carbon coils.

growth of the carbon coils with helical, spiral, threadlike, or twisted forms was very rare and extremely accidental, and the reproducibility was very poor. Thus the production was almost excluded as the helical/spiral or twisted form is unusual. Furthermore, the versatile potential applications of the carbon coils were not known and recognized in those days. The reproducibility of the growth of carbon coils from vapor phase was afterward outstandingly improved, and nowadays the carbon coil is semi-mass-produced. The growth mechanism of the VGCF with a straight form has been proposed by many researchers. It may be considered

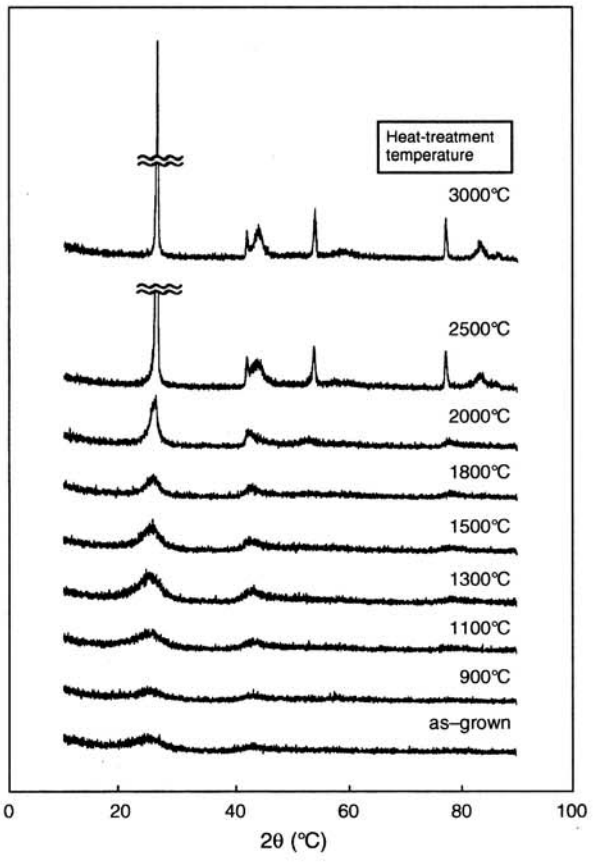

Figure 24. XRD patterns of as-grown and heat-treated carbon coils.

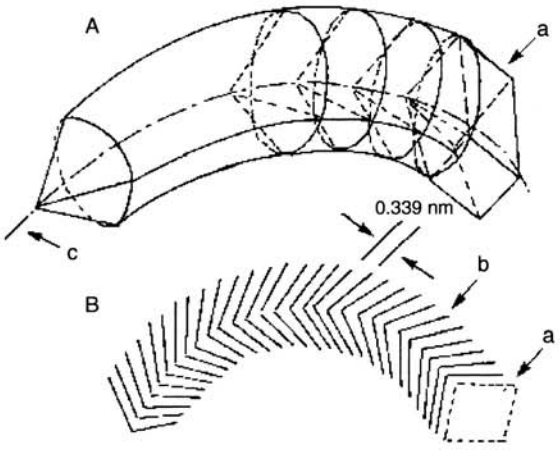

Figure 25. Schematic image of the herringbone structure of the graphite coil: (A) 3D image, (B) 2D image showing graphite layers. (a) Catalyst grain, (b) Graphite layers, (c) Fiber axis [82].

that the growth of carbon coils with various morphologies is the general growth pattern of a VGCF and a straight VGCF is the rather special case. Accordingly, the growth mechanism of the carbon coils has also been proposed by those researchers as well as the establishment of the preparation processes of the carbon coils.

In this section, the growth models or mechanisms of the carbon coils are reviewed.

2.6.1. Boehm's Mechanism

Boehm [14] proposed a schematic growth model of filamentary carbon on iron carbide with two active faces at oblique. He considered that if the catalyst particle has an angular shape as shown in Figure 26, a curved carbon fiber would grow from the active crystal faces due to the different diffusion path lengths in the carbide crystals resulting in the growth of helical growth forms if strands grow to any length, and double helices would result if two adjacent crystal faces are active.

2.6.2. Baker's Branching Mechanism

Baker and co-workers [17] obtained spiral carbon filaments from acetylene at above 800 °C using the Sn/Fe (Sn coated Fe foils) catalyst. Branching of carbon filaments was common as shown in Figure 27. They suggested the principle means of relieving the stress created by the fact that filaments were often forced against the mass of deposit in two directions, and when this stress became too great the particle was squeezed out from between these two filaments and began to propagate a new pair.

2.6.3. Baker's Filament Growth Model

Baker and Chludzinski [81] examined the effect of the various metal oxide additives to the Ni–Fe catalyst on the inhibition of the growth of carbon filaments using C_2H_2 as a source gas. Many filaments formed in the presence of TiO_2 (Ni–Fe/TiO_2 catalyst) were in a spiral conformation, where the catalyst particle was located within the filament, which grew from two faces of the particle in opposite directions.

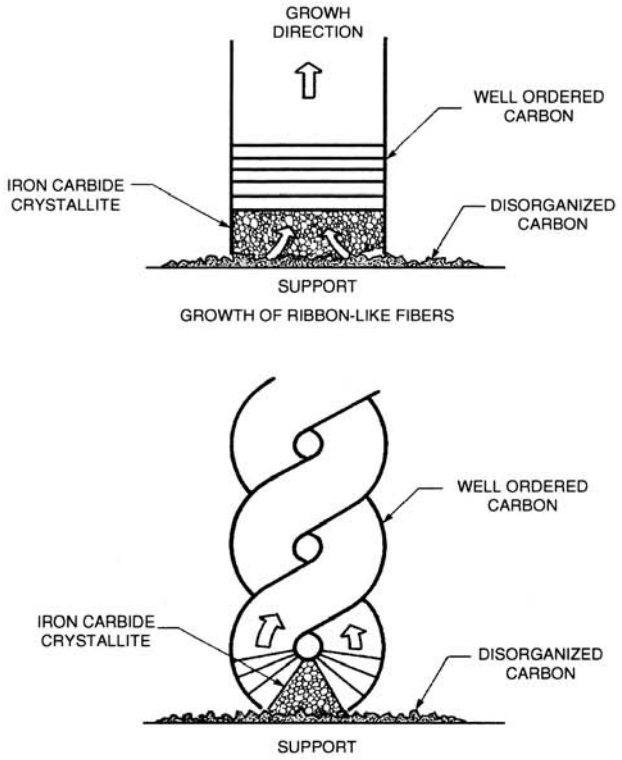

Figure 26. Schematics representation of growth mechanism of filamentary carbon on iron carbide (a) on rectangular carbide particle, (b) on carbide particle with two active faces at oblique angle [14, 29].

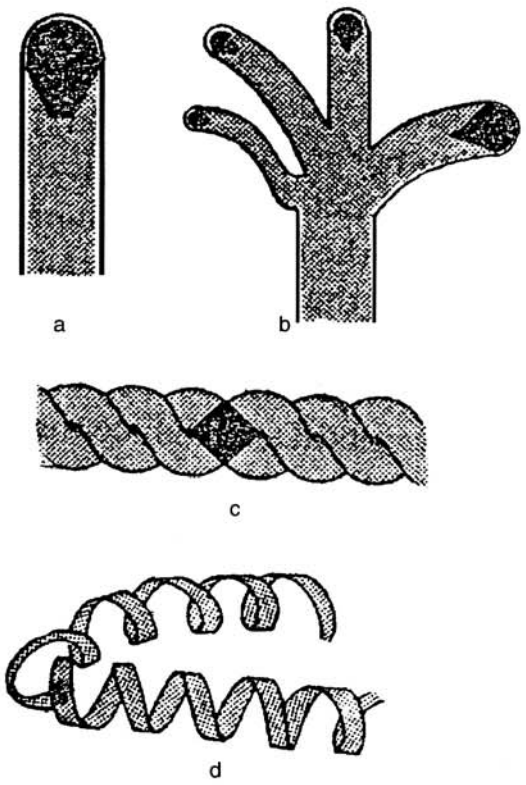

Figure 28. Schematic representation of different types of growth morphologies observed in carbon filaments [86]. (a) Whisker-like, (b) branched, (c) spiral, (d) helical.

2.6.4. Downs–Baker Mechanism

Downs and Baker [86] obtained various carbon filaments (e.g., branched, spiral, helical, with coil diameter of about 100 nm) using carbon fibers as the substrate as schematically shown in Figure 28. They also proposed the growth mechanism of the coils.

2.6.5. Kim–Baker Mechanism

Kim and co-workers [20] reported the growth of coiled carbon fibers using C_2H_2 and Cu/Ni(1:1) at 700 °C. Two filaments grew from opposite faces of the catalyst particles at identical rates. Furthermore, during the major part of the growth process, the filaments were relatively smooth and tended to form into large loops. The catalyst particles reached a size of about a third of the original value; they appeared to undergo a further change in shape and simultaneously started to rotate on an axis perpendicular to the direction of filament growth, causing the filament to acquire a spiral form. This action normally continued for a relatively short time, being the prelude to catalyst deactivation. This phenomenon was observed at all growth temperatures.

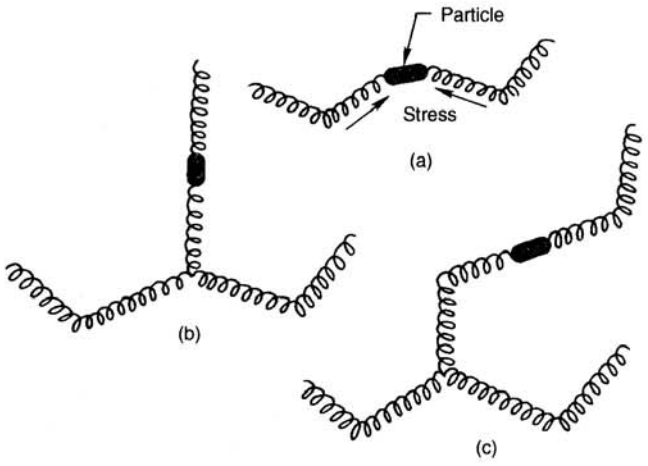

Figure 27. Bifilament morphology of coiled carbon fiber observed in the Sn/Fe system. [17, 29].

2.6.6. Amelinckx's Mechanism

Amelinckx and co-workers [31] examined in detail the different coiling morphologies of the graphite tubes grown by the Co-catalyzed decomposition of acetylene and proposed a new model based on the concept of the spatial-velocity hodograph to describe quantitatively the extrusion of a carbon tubule from a catalytic particle as shown in Figure 29. The coiled fibers were generally found to be hollow tubes consisting of concentric cylindrical graphene sheets. The tubules can adopt various shapes such as straight, curved, planar-spiral, and helix, often with a remarkably constant coil pitch. It is generally accepted that the tubules grow by the extrusion of carbon, dissolved in a metallic catalyst particle that is supersaturated in carbon at one part of the surface. The most detailed description of this growth process was given by Baker [87].

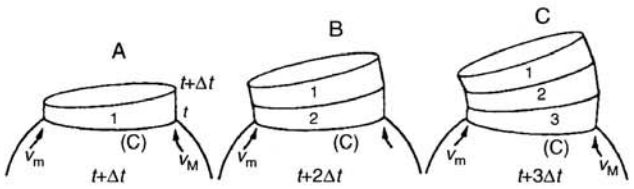

Figure 29. Successive stages in the extrusion of carbon according to the hodograph of the extrusion velocities for the case of a uniform bent tubule [31].

2.6.7. Owens's Mechanism

Although it is well known that sulfur acts as a poison for many Ni-catalyzed reactions, Owens and co-workers [28] observed that certain benefits of sulfur can be derived from following a partial and well controlled sulfidization treatment of the metal catalyst for the growth of carbon filaments by the nickel catalyzed decomposition of C_2H_4/H_2 mixtures. That is, the pretreatment of Ni in low levels of H_2S (4–50 ppm) results in a reconstruction of the metal surface and thus induces some major perturbations in the morphological characteristics of the filamentous carbon deposit to regularly form coils. This change in growth mode indicates that sulfur is modifying the diffusion characteristics of carbon species through the catalyst particle.

2.6.8. Fonseca–Dunlop Mechanism

Fonseca and co-workers [88, 89] reported a model of perfectly graphitizable coiled carbon nanotubes and discussed the growth mechanism of the coiled carbon nanotubes. The presence of a large amount of curved and coiled nanotubes among the straight tubes produced by the catalytic method stimulated several studies on the theoretical aspect of the coiling mechanism [88, 90–93]. It was proposed that the curving and coiling of the straight tubes can be accomplished by the occurrence of knees (i.e., two straight cylindrical tube sections of the same diameters connecting at an angle). Such knees can be obtained via the insertion in the plane of the knee of diametrically opposited pentagonal and heptagonal carbon rings in the hexagonal networks. The heptagon is on the inner side of the knee and the pentagon is on the outer side. The possibility of such a construction was predicted by Dunlap [94–96]. Theoretical models of curved nanotubes forming toroids of irregular diameters have also been described by Ihara and Itoh [97]. Fonseca suggested a growth mechanism on a catalyst at a molecular level using the heptagon–pentagon construction of Dunlap [95]. Dunlap explained the formation of curved nanotubes, tori, or coils by this concept. Dunlap also observed that the diameter range of the young tube (1 min) is about the same as that of the old ones (80 min). For a long time exposure (5 h) of the tubules to the reaction conditions, only amorphous carbon was deposited on the outer layer and no tubes with higher diameters were observed.

2.6.9. Li's Mechanism

Li and co-workers [98] obtained coiled nanotubes by the Fe-catalyzed pyrolysis of acetylene at 973 K and examined the morphology and microstructure in detail. The obtained coil was a single coil and has a 70 nm coil diameter and a 130 nm coil pitch. It was suggested that the formation of the coiled nanotubes was due to the mismatch between the extrusion velocity by the catalyst particle and the rate of carbon deposition.

2.6.10. Motojima's Anisotropy Mechanism

Motojima and co-workers [1, 50, 99] proposed the two- and three-dimensional growth mechanism of the carbon coils based on the anisotropic deposition of carbon on the different catalyst crystal planes. Figure 30 shows the tip part of the carbon coils obtained in an initial growth stage. It can be seen that two carbon fibers grew from a catalyst grain (white part) and curled to from double coils. Figure 31 shows the schematic 2D-growth model. If the catalytic activity of a crystal plane A of a catalyst grain is larger than that of B, the grown fiber will be curled to the right direction to form carbon coils. On the other hand, if there is no difference in catalytic activity between crystal planes A and B, a straight carbon fiber grows. Figure 32 shows the 3D-growth model. Six carbon fibers grew basically from six crystal planes following coalescence to form two fibers. That is, one fiber is formed from fine carbons deposited from three crystal planes, in which three crystal faces may have different catalytic activities. Motojima and co-workers [45, 99] have found that a different crystal face of a Ni single crystal has different catalytic activity for the growth of carbon coil, and the coil yield was 10.2% for Ni(100), 6.7% for Ni(111), and 3.2% for Ni(110). Circular carbon coils with circular fiber cross section are predominantly formed during the initial growth stage and then change to flat coils with increasing reaction time because of the change in the catalyst shape from cubic to slender form. A change in the catalyst form may be effected by the electromagnetic field (force) emitted from the outer electric heater as schematically shown by Chen and co-workers [100]. Yang and Chen [101] reported that for the carbon filament growth using the Ni-catalyzed pyrolysis of methane at 700 °C, the most preferable crystal plane for graphite precipitation was Ni(111) followed by Ni(111) > (311) > (100) > (110). Accordingly, the grown carbon fiber curls such that the fiber plane deposited from higher catalytic plane is outer part of the curled fibers to

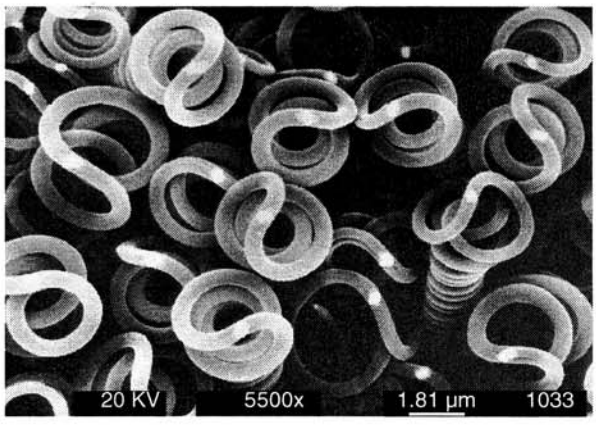

Figure 30. Tip of the carbon coils grown on a Ni catalyst in the initial reaction stage [63].

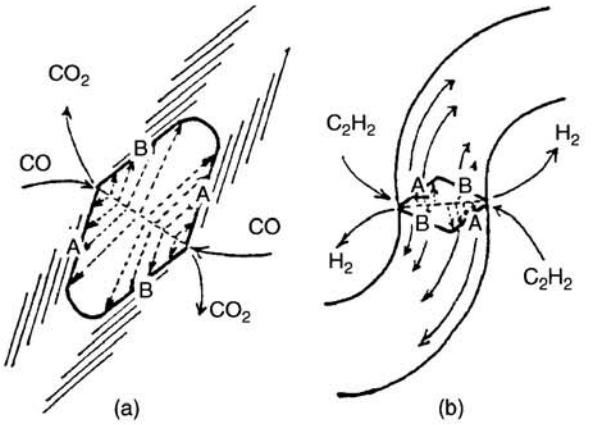

Figure 31. 2D-schematic growth model of (a) straight carbon fiber and (b) carbon coil [136].

from carbon coils. The coil diameter is determined by the difference in catalytic activities of A and B, and coil pitch by the difference in B and A or C.

2.6.11. Chesnokov's Mechanism

Chesnokov and co-workers [27] proposed the growth mechanism of the symmetrical helical filamentous carbon fibers obtained by the decomposition of butadiene-1,3 over Ni–Cu/MaO catalyst at 723 K. Figure 33 shows the schematic growth model. In the initial growth stage, butadiene-1, 3 decomposes to form carbon and hydrogen atoms. Carbon atoms diffuse into the Ni/Cu alloy bulk and gradually oversaturate to nucleate and form metastable Ni_3C on the frontal side of the alloy particle. Planes (111) of Ni/Cu alloy are the most preferable for the graphite nucleation since graphite (002) and alloy (111) planes, which determine the filament growth direction, are similar in symmetry and interatomic distances [27]. Intensive carbon atom diffusion flow toward the crystallization center then occurs, which results

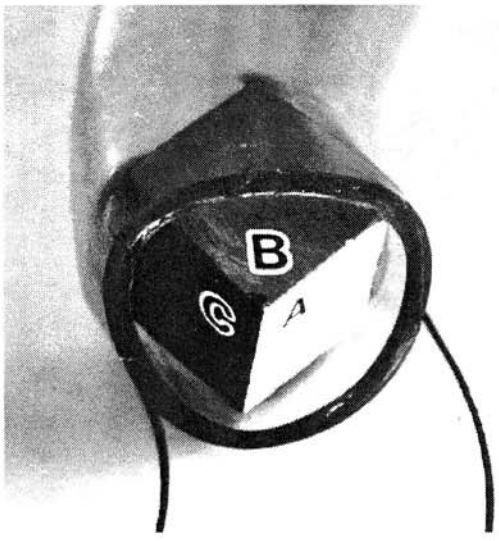

Figure 32. 3D-schematic growth model of carbon coils [1]. A, B, and C show the different crystal faces.

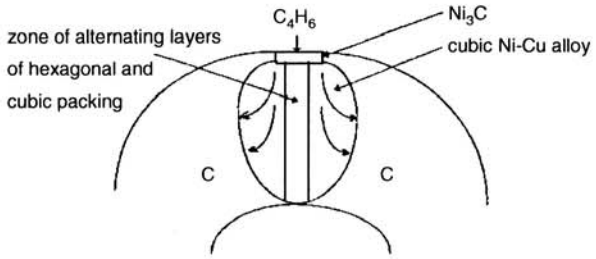

Figure 33. Schematic diagram of the growth mechanism of helix filamentous carbon produced from butadiene-1,3 on Ni–Cu crystals [27].

in dislocation of metal atoms and thus distorts the spherical shape of the particle to an elongated form. As can be seen in Figure 23, different carbon atoms pass via unequal diffusion from the places where they enter the alloy particle through the Ni_3C phase to different surface patches where graphite phase grows. This results in different growth rates and filament twisting [27].

2.6.12. Chiral Nanotube

Liu and Cowley [102] reported on the electronic structure of chiral nanotubes. Akagi and co-workers [103] studied general features of the electronic states of helically coiled cages of graphite layers by simple tight-binding models. Ihara and Itoh [97] reviewed the recent status of research of helical and toroidal forms, which contain pentagons, hexagons, and heptagons of carbon atom. Figure 34 shows the schematic model of a helically coiled form of C_{360}. The atomic arrangements of the structures of the helically coiled forms of the carbon cage for the single layer, which are found to be thermodynamically stable by molecular-dynamics simulations, are compared to those of the experimentally helically coiled forms of single and multilayers graphite forms that recently have been experimentally observed.

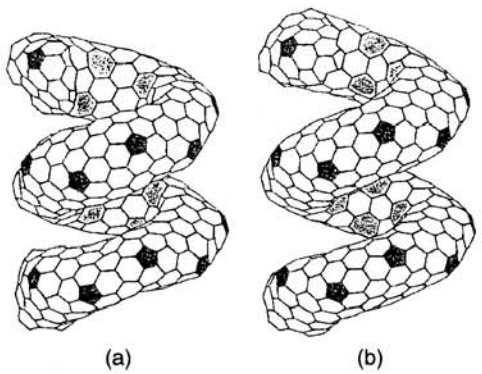

Figure 34. Helically coiled form C_{360} [97]. One pitch contains a torus C_{360}. (a) Coil length = 12.9 Å and (b) coil length = 13.23 Å. The tiling pattern of heptagons in the inner ridge line is changed, though the pattern of pentagons in the outer ridge line remains upon changing the coil length.

2.7. Properties

2.7.1. Mechanical Properties

The mechanical properties of the carbon coils were evaluated in detail by Motojima and co-workers [46, 104–108]. The circular carbon coils with a circular fiber cross sections and with large coil diameter can extended elastically up to 4.5–15 times original coil length, while flat coils with flat or rectangular fiber cross sections can only be extended up to 1.5 times the original length. For example, the carbon coil can be extended to nearly straight form as shown in Figure 35 [108]. The carbon coils extends linearly with increasing applied load. The rupture strength of the as-grown carbon coils is 42–114 MPa. The rigidities of the circular and flat as-grown carbon coils are 22–46 GPa and 22–33 GPa, respectively.

2.7.2. Electric Properties

The bulk (powder) electrical resistivity of the as-grown carbon coil decreases with increasing the bulk density and is 1–10 π/cm for bulk density 0.3 g/cm^3 and 0.1–0.2 π/cm for 0.6 g/cm^3 as shown in Figure 36 [82]. The resisitivity of the bulk carbon coils can be decreased steeply with the surface coating by carbon [83], TiC [109], TiN [110], ZrC [104], NbC [111], and TaC [112] but not by graphitizing at high temperature heat treatment [82]. Kaneto and co-workers [113, 114] examined the electrical conductivity of the carbon coils in detail. The electrical conductivity along the helical axis of a piece of carbon coil is 30–100 S/cm. This conductivity is rather small compared with multiwalled carbon nanotubes. Figure 37 shows the current–voltage (i–v) curve of a piece of carbon coil. The (i–v) characteristics indicate that the current shows superlinear dependence on the applied voltage at high fields. The fact is explained by heating of the coil by electrical power, because of the higher conductivity at higher temperature, or the high field effect. The temperature dependence of conductivity showed that one of the possible transport mechanisms is the 3D variable range hopping model. Kaneto and co-workers [114] also examined the electrical conductivities of the carbon coils under various gas atmospheres. The conductivity of a single coil increased by 5–20% upon evacuation for several minutes. Furthermore,

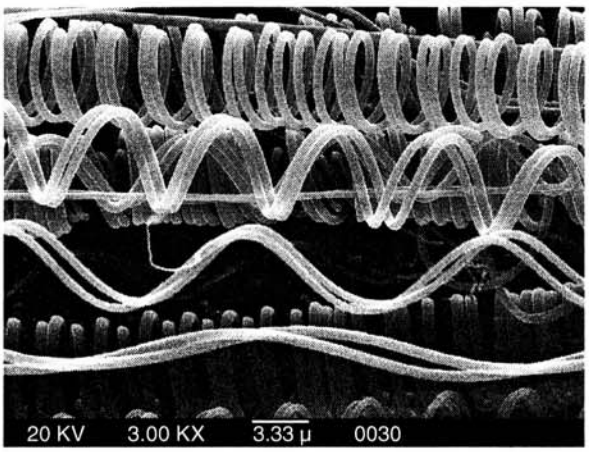

Figure 35. Extended carbon coils [108].

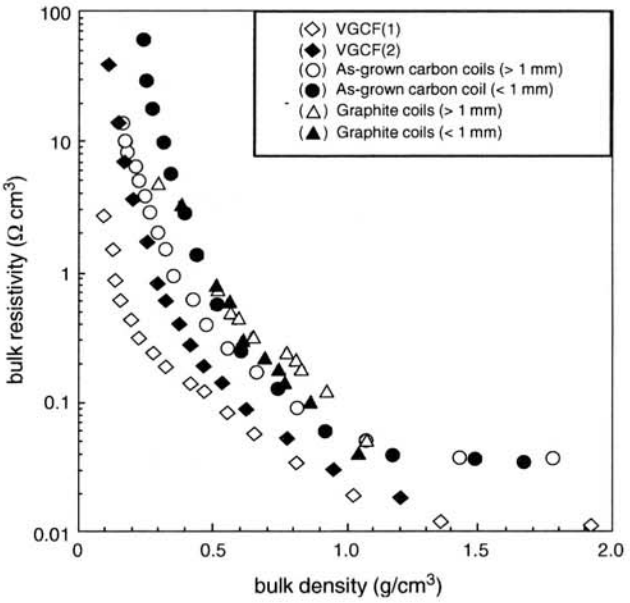

Figure 36. Bulk electrical resistivity obtained at room temperature in air [82].

the conductivity increased by 1–2% upon exposure to iodine (oxidative) gas for several minutes. On the other hand, upon exposure to ammonia (reductive) gas from the vacuum, the conductivity decreased nearly to the same value of the air atmosphere. However, the degree of conductivity was found to be small compared with the case of other π conjugated systems such as conducting polymer.

Fujii and co-workers [115, 116] examined the magnetoresistance of the as-grown and heat-treated carbon coils in the magnetic field in the range from 0 to 12 Tesla at 290 K. The magnetoresistance of the as-grown carbon coil does not change under strong magnetic field up to 12 Tesla. On the other hand, the magnetoresistance is negative for specimens

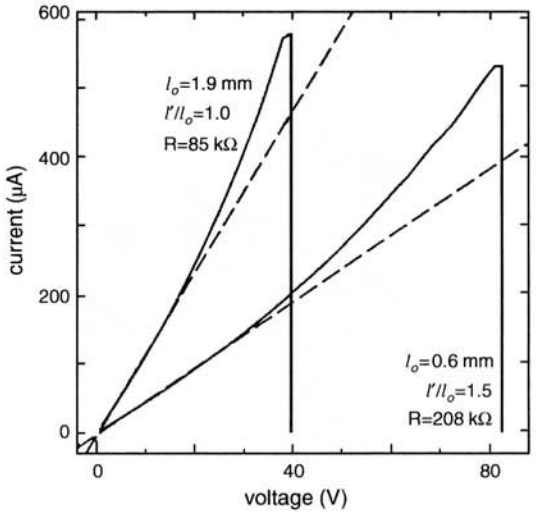

Figure 37. Voltage–current (i–v) characteristics of a carbon coil [113, 114]: l_o: coil length before stretch, l: coil length after stretch, R: electrical resistivity.

heat-treated at 1500 °C and 2000 °C and positive for specimens heat-treated at 2500 °C and 3000 °C. The absolute value of the magnetoresistance ratio $\{R(B) - R(0)\}/R(0)$ increased with increasing magnetic field, 40% at parallel magnetic field of 12 T, and 5% at 5 T, and 14% under transverse magnetic field of 12 T as shown in Figure 38.

2.7.3. Field Emission Properties

Pan and co-workers [117] reported on the field emission properties of carbon tubule nanocoils. The carbon nanocoils show the low turn-on field of 180 V at a 130 μm gap and high emission current of 10^{-3} A/cm^2 at 300 V as shown in Figure 39 and also shows excellent stability of emission for over 250 hr. These values are sufficient for commercializing the carbon-nanofiber-based field emission displays. Accordingly, the carbon nanocoil is expected to be a novel attractive candidate for the fabrication of flat panel field emission displays.

2.7.4. Electromagnetic Properties

It is considered that the carbon coil is a promising candidate as a novel EM wave absorber, especially in the GHz range, because of its microcoiling morphology. That is, the microcoiling morphology is the most effective and ideal one for the generation of inductive current by Faraday's law resulting in absorption of EM waves. Actually, the carbon coils can absorb EM waves in the GHz region without reflection. Motojima and co-workers [47, 83, 118–120] examined the absorption ability (reflection loss) of EM waves, especially in the GHz regions, in detail. The as-grown carbon coils can strongly absorbed the EM waves of 13.9 and 16.3 GHz, and the reflection loss is below −40 dB (99.99% absorption). The absorption region can be broadened by addition of other additives. Figure 40 shows the reflection loss of the CMC-containing PMMA (polymethylmetacrylate) beads for 75–105 GHz regions. It can be seen that the reflection loss below −30 dB (99.9% absorption) of EM waves can be obtained by only 1 wt% addition in the PMMA beads.

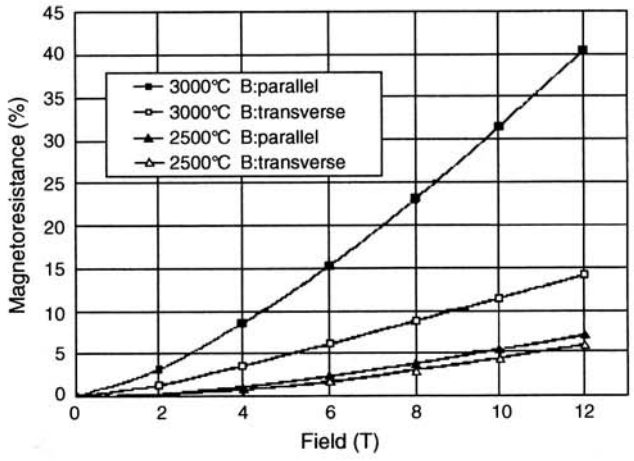

Figure 38. Effect of magnetic field on the magnetoresistance of a heat-treated carbon coil (graphite coil): Temperature: heat-treated temperature. Parallel and transverse: the direction of magnetic field is parallel and transverse (vertical) to the coil axis, respectively [116].

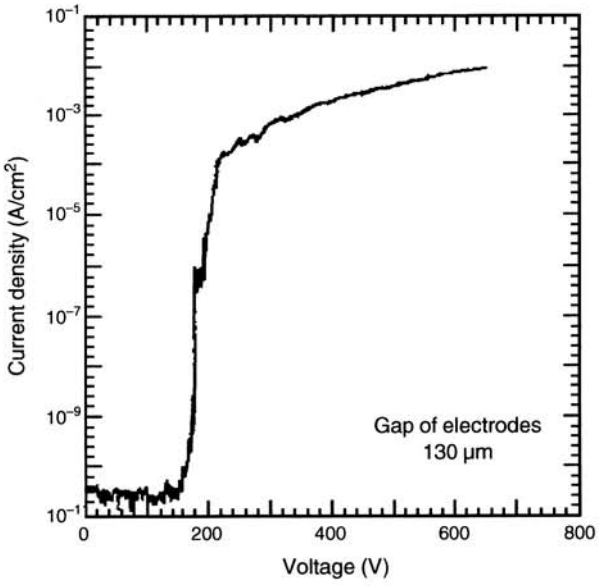

Figure 39. Curve of the emission current density vs applied voltage for a typical nanocoil field emitter [117]: The low turn-on voltage and high current density are obtained.

The higher addition above 2 wt% or lower addition below 0.5 wt% results in lower reflection loss. Du and co-workers [121] examined microwave electromagnetic characteristics of a microcoiled carbon fiber/paraffin wax composite in Ku band frequencies (12.4–18 GHz).

2.7.5. Chemical Properties

The carbon coil become oxidized at about 450 °C in air, and the weight significantly decreases with increasing temperature and burn out at 700 °C [122]. On the other hand, the graphite coils obtained by the heat treatment of as-grown carbon coils at 3000 °C for 6 hr in $CO + CO_2$ become oxidized at about 700 °C in air. The oxidation behaviors of the as-grown and heat-treated carbon coils are examined in detail to improve the surface inertness and enhance the

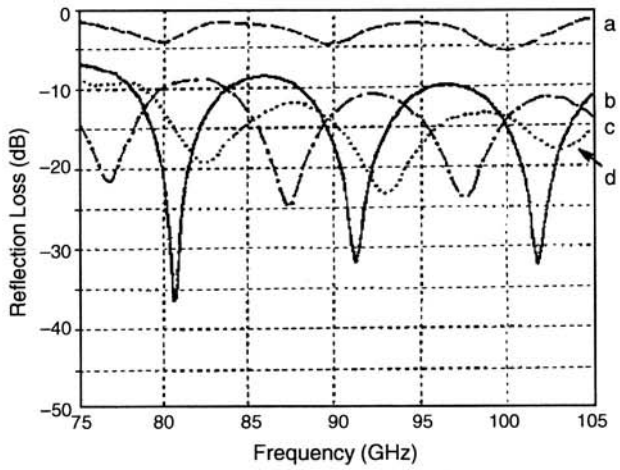

Figure 40. Reflection loss of the CMC-impregnated PMMA bead. CMC content: (a) 0 wt%, (b) 1 wt%, (c) 2 wt%, (d) 3 wt%.

chemically active sites [54, 122, 123]. The graphite coil is stable up to about 1200 °C in Ar atmosphere. However, the graphite coil is partially oxidized by the small amount of oxygen impurity included in Ar at the contact part of two graphite layers in which large inner stress may be impressed to form on amorphous state. Shibagaki and Motojima [54, 123] examined in detail the partial oxidation characteristics of the surface of the carbon coils, under low O_2 flow rate at 450–820 °C to improve the surface chemical activities.

2.7.6. Thermal Properties [82, 106, 123]

The carbon coils can be heat-treated up to 1000–3000 °C in $CO + CO_2$, Ar, or N_2 atmosphere to form graphite coils with full preservation of the coiling patterns of the carbon coils. The elasticity of the as-grown carbon coils is reduced by the heat treatment and became brittle. The ruptured cross section of the fiber which composes the circular graphite coil takes either a trigonal pyramid-like form or a negative pyramidal hollow. On the other hand, the ruptured cross section of the flat graphite coils either has rooflike extrusion or is hollow. These characteristic patterns suggest a growth mechanism of the carbon coils. Many distinct striations, declined at 40–50 deg against fiber axis, can be seen on the surface. The TEM image of the tip part of the ruptured fibers shows that distinct graphite layers ($d = 0.339$ nm) are developed with an inclination of 35–40 deg versus the fiber axis to form a "herringbone" structure. The lattice parameter is $a = 0.2464$ nm and $c = 0.6772$ nm. The "c" value is slightly larger than the reported value for graphite of 0.6714 nm while the a value is the same as that of graphite ($a = 0.2463$ nm). Raman spectra show that the graphite layers of the graphite coils are not more developed than the 100–200 μm long VGCF. This may be caused by the presence of some disorders in the graphite layers and/or the smaller submicrometer width of the graphite layers in the graphite coils.

3. CERAMIC NANOCOILS/NANOTUBES

3.1. Introduction

Ceramic materials with a 3D nanocoiled or nanotubed structure (referred to as "ceramic coils" hereafter) are not commercially available. Ceramic coils are very interesting as new functional materials with many potential applications, such as light weight thermal barriers, heat exchangers, gas separation materials, absorbers for electromagnetic waves, microsensors, electrodes materials, catalysts, etc. The growth of various coiled ceramic fibers by CVD process has sometimes been observed with mixing straight fibers so far. These coiled fibers are generally very irregularly coiled, and the growth is extremely accidental and without reproducibility. On the other hand, Motojima and co-workers [9, 10, 124, 125] first found that very regularly coiled silicon nitride (Si_3N_4) fibers could be obtained with good reproducibility by the CVD process. After then, they prepared various ceramic coils such as metal carbides, nitrides, and oxides using a carbon coil as a template with high yield. Growth of various ceramic coils by the CVD process, electroplating, or the biomimetic process has also been reported by some researchers.

In this section, preparation, morphology, growth mechanism, and some properties of various ceramic coils/tubes are reviewed.

3.2. SiC and Si_3N_4

The vapor growth of the helical SiC fibers was first reported by Addamiano [126]. He found that the coiled crystals of 2H-SiC grew in mixing in a mass of straight 2H-SiC whiskers during the hydrogen reduction of methyltrichlorosilane at 1400–1430 °C on graphite substrate. After then, Kang and co-workers [127] reported that irregularly coiled SiC whiskers grew among the straight or irregularly curled SiC fibers during the carbothermal reduction of SiO_2 by carbon at 1500 °C under Ar + CO atmosphere. The springlike SiC whiskers did not grow in the presence of Fe impurity but grew in NaCl impurity. It was suspected that the formation of the springlike whiskers should be closely related to the presence of chlorine impurity.

Motojima and co-workers [68] prepared the SiC coils using a powder mixture of SiO and cooked rice husks at 1400–1450 °C. The SiC coils were triple coils with a 0.5–1 μm coil diameter and a 10–100 μm coil length. Motojima and co-workers [47, 106, 128, 129] also easily prepared the SiC coils by the vapor phase diffusion process using a carbon coil as a template.

Motojima and co-workers [9, 10, 124] first prepared very regularly coiled silicon nitride (Si_3N_4) fibers by the Fe-catalyzed CVD process using a $Si_2Cl_6 + NH_3$(or N_2) + H_2 gas mixture at 1200 °C on a graphite substrate. The Si_3N_4 coils are single-helix coils and have a coil diameter of 10–15 μm and a coil pitch of 3–5 μm as shown in Figure 41. The coils have a crystalline Si_3N_4 core surrounded by an amorphous Si_3N_4 clad [130] and have excellent elastic and mechanical properties [26, 131–133]. Iwanaga and co-workers [134] review the ceramic microcoils including the Si_3N_4 coils. Vogt and co-workers [135] prepared the microcoiled Si_3N_4 fibers by the reaction of SiO_2 with NH_3 at 1400 and found that addition of Fe and W impurity in SiO_2 partly promotes the growth of the microcoiled Si_3N_4 fibers. The Si_3N_4 coils obtained by them are single-helix coils with a fiber diameter of 2–10 μm and a coil diameter of 5–20 μm.

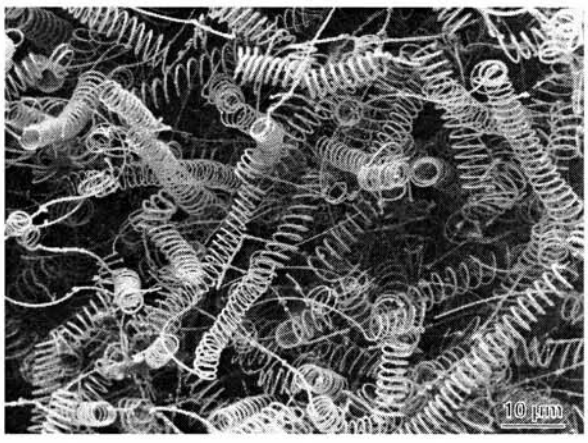

Figure 41. Si_3N_4 microcoils prepared by a Fe-catalyzed CVD process [9, 10].

3.3. TiC, TiN

Motojima and co-workers [136] prepared a TiC microcoil by the CVD process using a source gas mixture of $TiCl_4 + H_2 + PCl_3$ and a Si + Pd catalyst dispersed on a graphite substrate at 1050 °C. The TiC coils were double-helix coils similar to DNA and have a coil diameter of 1–5 μm and a coil length of 20–150 μm. Motojima and co-workers [47, 109, 128, 129, 137] also obtained TiC coils by a vapor phase diffusion process (titanizing or nitriding) using carbon coils as the template, with full preservation of the coiling morphology of the source carbon coils. The bulk (powder) electrical resistivity of the TiC coils decreased with increasing titanizing ratio and attained 0.01Ω cm at a bulk density of 1.4 g/cm^3. Addition of the N_2 or NH_3 gases resulted in the formation of TiN microcoils because the nitride phase is thermodynamically more stable than the carbide phase.

3.4. ZrC, ZrN

Motojima and co-workers [104, 129] prepared ZrC and ZrN coils by the vapor phase diffusion process using the carbon coils as a template. Depending on the reaction conditions, ZrC/C(carbon coil)/ZrC composite coils to a single phase ZrC coil could be obtained, with full preservation of the coiling morphology of the carbon coil and coil yield 100%. Addition of N_2 or NH_3 gases in the reaction atmosphere resulted in the formation of ZrN coils.

3.5. NbC, NbN, TaC, TaN, HfC

Motojima and co-workers [47, 106] obtained NbC coils by the vapor phase diffusion process using the carbon coils as the template. Depending on the reaction conditions, NbC/C(carbon coil)/NbC composite coils to single phase NbC coils could be obtained, with full preservation of the coiling morphology of the carbon coil and coil yield 100%. Addition of the N_2 or NH_3 gases resulted in the formation of a ZbN/C(carbon coils)/NbN–NbN coils/tubes [138, 139]. The carbides or nitrides of Ta or Hf were also obtained using similar processes [47, 106, 112, 116, 129, 138].

3.6. SiO_2, TiO_2

Robbie and co-workers [9, 140] found that porous and chiral films of SiO_2 could be obtained by the GLAD (glancing angle deposition) process using electron-beam evaporation onto the glass substrates coated with an ITO transparent conductor. They showed that using the GLAD process, the microstructure parameters such as helical rise angle, pitch, and handedness could easily be controlled, and structures such as pitch gradients and stacked layers of different pitch and/or handedness were also easily produced. For example, the pitch in a helical GLAD films can be controlled by the ratio of deposition rate to substrate rotation rate, while the handedness can be controlled by the direction of rotation. Figure 42 shows an example of a chiral GLAD SiO_2 film [141]. This film has left-handed helical columns with 8.4 turns and pitch $p = 410$. Robbie and co-workers [140, 142] also obtained chiral liquid crystal films by embedding LC into the porous and chiral SiO_2 films. Helical/spiral forms are also frequently observed in materials such quartz

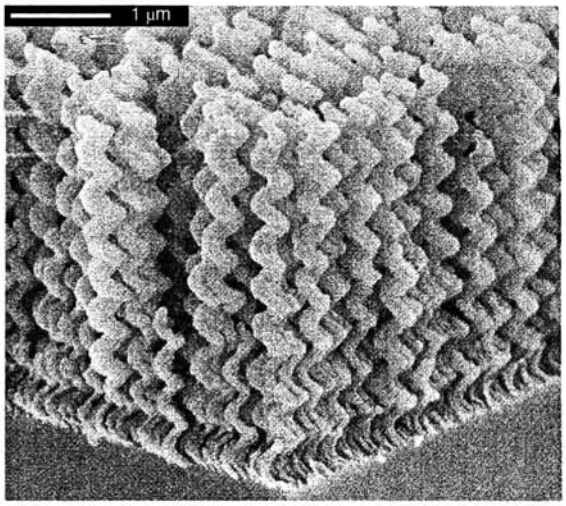

Figure 42. Example of a chiral GLAD SiO_2 film [140]. A left-handed helical film with 8.4 turns of pitch 410 nm is shown. The film pitch is the thickness of one turn of the helix and relates to the wavelength at which peak chiral optical activity is observed.

[143]. Yang and co-workers prepared hollow helicoids made of hexagonal mesoporous silica [144]. Research group of Shinkai studied the preparation of silica fibrils with a novel double stranded helical structure by sol–gel transcription of twisted bilayer ribbons formed by cationic gemini surfactants [145]. Motojima and co-workers [146] prepared TiO_2 microcoils/tubes by sol–gel and CVD processes using a carbon coils as a template as shown in Figure 43.

3.7. Miscellaneous

Gleize and co-workers [147] prepared tubular BN fibers with a helical form by a CVD process using $B_2H_6 + NH_3$ (or N_2) at 1100 °C using the ZrB_2 catalyst. The thickness of tubular fiber is 0.1 μm, coil diameter is 0.2 μm, and coil length is 5 μm. Johansson and co-workers [148] proposed a

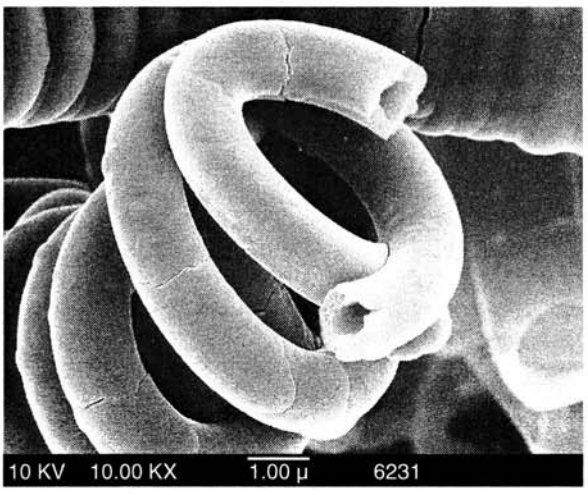

Figure 43. TiO_2 helical coils obtained using a carbon coils as a template.

new method for the preparation of three-dimensional structures in free space, a laser-assisted CVD process with a high-resolution micropositioning system. In this process, a linear three-axis micropositioning system and laser beam which was focused on the tip of the growing point are used. Using this process, they prepared a 3D-boron spring with spring diameter of 350 μm from a gas mixture of $BCl_3 + H_2$ gas mixture. This boron spring has high mechanical properties such as an elastic modulus of 420–450 GPa, fracture strain of 2.7–3.7%, and a fracture stress of 12–17 GPa. Jiang and co-workers prepared AN whiskers with wavy (helical) structure by the SHS (self-propagating high-temperature synthesis) method [149]. The growth of helical fibers of GaP[150], GaAs[151, 152], MnAs[153], ZnS[151], Cu[154], Cu–Zn[154], and $(SrBa)CO_3$ [155] from a vapor phase was also reported. Furthermore, the helical calcium carbonates, barium sulfate, and silica were also prepared by the biomimetic process [156–160].

4. APPLICATIONS

Downs and Baker [86] first predicted that the unique structural conformations of helical form which can frequently be found in vapor grown carbon filaments will open up numerous possibilities in the fabrication of new functional materials. Lakeman and co-workers [159] prepared microcoiled carbon fibers with coil diameters of several hundred micrometer and coil pitches of about 100 μm for the application to the semiconducting infrared detection elements. Pan and co-workers [117] showed that the carbon nanocoils are expected to be novel attractive candidates for the fabrication of a flat panel field emission display. Motojima and Iwanaga [118] showed that the carbon coils have an excellent EM absorption ability, especially in GHz regions. The helical carbon coils will have versatile applications such as EM absorbers, field emitters, hydrogen absorption–desorption materials, energy exchanging materials, tunable microdevices, microsensors, microactuators, micromachines, chiral catalysts, extend-contractable electrodes, reinforcements for soft and/or extendable materials, hydrogen storage materials, activators for organisms, etc.

GLOSSARY

Carbon microcoil Carbon microcoil (CMC) is a kind of vapor grown carbon fiber obtained by the catalytic pyrolysis of hydrocarbons or disproportionation of CO. The CMC generally has the double-helix coiling morphology similar to DNA, and has a coil diameter of 1–50 μm and a coil length of 0.1–20 mm. The as-grown CMC is almost amorphous and has no pore (tube) in the fiber axis.

Carbon nanocoil Carbon nanocoil (CNC) has the generally single-helix morphology with a small coil diameter of 10–500 nm.

Ceramic microcoil Ceramic microcoil is generally tuberous ceramic fibers with 3D herical/spiral structure and coil diameter of micrometer order, and can be prepared directly by the chemical vapor deposition (CVD) process, or indirectly by the sol–gel or CVD processes using carbon microcoils/nanocoils or chiral polymers as the templates.

Coiling-chirality "Chirality" is generally used in the mean of optical iromerism (enantiomer) with mirror-symmetry of *levo*-rotatory (*l*) and *dextro*-rotatory (*d*). On the other hand three dimensional chiral/coiling morphology has two kind of coiling patterns, right clockwise and left clockwise coiling patterns in mirror symmetry, and they are not superimposed with each other. Accordingly, two kinds of coiling patterns are referred to as a coiling-chirality.

Cosmomimetic carbon coil Three dimensional (3D) helical/spiral structures are commonly observed in all objects in cosmos, nature, living bodies, electromagnetic waves, economic cycles, etc. That is, 3D helical/spiral structure is a fundamental structure in all things in the cosmos. Accordingly, the carbon microcoils or nanocoils with 3D helical spiral structure is referred to as "cosmomimetic carbon coil" after the term of "biomemetics".

Helix, spiral, coiling "Helix" is used mainly in the field of living polymers such as DNA or protein, or synthetic polymers, while the terms of "spiral", "coiling" or "screw" are used in the fields of general substances or materials. The terms of helix, spiral and coiling represent the same means of the three dimensional forms or morphologies such as springs, coils, screws, whirlpools, vortex, etc.

REFERENCES

1. S. Motojima and X. Chen, *J. Appl. Phys.* 85, 3919 (1999).
2. J. R. Winker and H. B. Grey. *Acc. Chem. Res.* 31, 698 (1998).
3. B. I. Yokobson and R. E. Smalley, *Am. Sci.* 85, 324 (1997).
4. N. M. Rodriguez, *J. Meter. Res.* 8, 3233 (1993).
5. K. P. de Jong and J. W. Geus, *Catal. Rev. Sci. Eng.* 42, 481 (2000).
6. W. R. Davis, R. J. Slawson, and G. R. Rigby, *Nature* 171, 756 (1953).
7. W. R. Davis, R. J. Slawson, and G. R. Rigby, *Trans. Brit. Ceram. Soc.* 56, 67 (1957).
8. S. Motojima, M. Kawaguchi, K. Nozaki, and H. Iwanaga, *Appl. Phys. Lett.* 56, 321 (1990).
9. S. Motojima, *Nature* 339, 179 (1989).
10. S. Motojima, S. Ueno, T. Hattori, and K. Goto, *Appl. Phys. Lett.* 54, 1001 (1989).
11. S. Motojima, S. Ueno, T. Hattori, and H. Iwanaga, *J. Cryst. Growth* 96, 383 (1989).
12. M. Hillert and N. Lange, *Z. Krist.* 111, 24 (1958).
13. R. T. K. Baker, M. A. Barbber, P. S. Harris, F. S. Feates, and R. J. Waite, *J. Catal.* 26, 51 (1972).
14. H. P. Boehm, *Carbon* 11, 583 (1973).
15. C. Park and R. T. K. Baker, *J. Catal.* 179, 361 (1998).
16. C. Park and R. T. K. Baker, *J. Catal.* 190, 104 (2000).
17. R. T. K. Baker, P. S. Harris, and S. Terry, *Nature* 253, 37 (1975).
18. R. T. K. Baker and R. J. Waite, *J. Catal.* 37, 101 (1975).
19. J. Galuszka and M. H. Back, *Carbon* 22, 141 (1984).
20. M. S. Kim, N. M. Rodriguez, and R. T. K. Baker, *J. Catal.* 134, 253 (1992).
21. N. Krishnankutty, C. Park, N. M. Rodriguez, and R. T. K. Baker, *Catal. Today* 37, 295 (1997).
22. C. A. Bernardo, I. Alstrup, and J. R. Rosytup-Nielsen, *J. Catal.* 96, 517 (1985).
23. M. T. Tavares, C. A. Bernardo, I. Alstrup, and J. R. Rosytup-Nielsen, *J. Catal.* 100, 545 (1986).
24. W. J. Jong, S. H. Lai, K. H. Hong, H. N. Lin, and H. C. Shih, *Diamond Relat. Mater.* 11, 1019 (2002).
25. K. Hernadi, A. Fonseca, J. B. Nagy, D. Bernaerts, and A. A. Lucas, *Carbon* 34, 1249 (1996).

26. N. Grobert, M. Terrones, S. Trasobares, and K. K. Ordatos, *Appl. Phys. A* 70, 175 (2000).
27. V. V. Chesnokov, V. I. Zaikovskii, and R. A. Buyanov, *J. Mol. Catal. A* 158, 267 (2000).
28. W. T. Owens, N. M. Rodriguez, and R. T. K. Baker, *Catal. Today* 21, 3 (1994).
29. J. L. Figueiredo, C. A. bernardo, R. T. K. Baker, and K. J. Huttinger, "Carbon Fiber Filaments and Composites," pp. 1–163, 405–439. Kluwer Academic, Dordrecht, 1990.
30. N. M. Rodoriguez, M. S. Kim, F. Fortin, I. Mochida, and R. T. K. Baker, *Appl. Catal. A* 148, 265 (1997).
31. S. Amelinckx, X. B. Zhang, D. Bernaerts, X. F. Zhang, V. Ivanov, and J. B. Nagy, *Science* 265, 635 (1994).
32. J. M. Mao and S. S. Xie, *J. Mater. Sci. Lett.* 18, 1151 (1999).
33. P. E. Anderson and N. M. Rodriguez, *J. Mater. Res.* 14, 2912 (1999).
34. F. Cesar, J.-O. Bovin, and L. R. Wallenberg, *J. Mater. Res.* 15, 1857 (2000).
35. M. Zhang, Y. Nakayama, and L. Pan, *Jpn. J. Appl. Phys.* 39, 1242 (2000).
36. L. Pan, M. Zhang, A. Harada, Y. Takano, and Y. Nakayama, *Amer. Inst. Phys. Conf. Proc.* 590 (2001).
37. L. Pan, T. Hayashida, A. Harada, and Y. Nakayama, *Physica B* 323, 350 (2002).
38. C. J. Lee, T. J. Lee, and J. Park, *Chem. Phys. Lett.* 340, 413 (2001).
39. X. Wang, Z. Hu, Q. Wu, X. Chen, and Y. Chen, *Thin Solid Films* 390, 130 (2001).
40. J. Xie, P. K. Sharma, V. V. Varadan, V. K. Varadan, B. K. Pradhan, and S. Eser, *Mater. Chem. Phys.* 76, 217 (2002).
41. K. Hernadi, A. Fonseca, J. B. Nagy, Á. Fudala, D. Bernaerts, and I. Kiricsi, *Appl. Catal. A* 228, 103 (2002).
42. J. B. Bai, *Mater. Lett.* 57, 2629 (2003).
43. T. Schliermann, G. Reichenauer, M. Thierley, B. Schmidt, and M. Glora, in "Proc. of Carbon 2002," Beijing, 201.
44. K. Hernadi, A. Fonseca, J. B. Nagy, A. Fudala, D. Bernaerts, and I. Kiricsi, *Appl. Catal. A* 228, 103 (2002).
45. X. Chen, S. Yang, and S. Motojima, *Mater. Lett.*, in press.
46. S. Motojima, M. Hirata, and H. Iwanaga, *J. Chem. Vapor Deposition* 3, 87 (1994).
47. S. Motojima, T. Hamamoto, N. Ueshima, Y. Kojima, and H. Iwanaga, *Electrochem. Soc. Proc.* 97-25, 433 (1997).
48. X. Chen and S. Motojima, *J. Mater. Sci.* 34, 5519 (1999).
49. M. Kawaguchi, K. Nozaki, S. Motojima, and H. Iwanaga, *J. Cryst. Growth* 118, 309 (1992).
50. S. Motojima, X. Chen, W. In-Hwang, T. Kuzuya, K. Kohda, and Y. Hishikawa, *Electrochem. Soc. Proc.* 13, 379 (2000).
51. S. Motojima, X. Chen, W. In Hwang, and Y. Hishikawa, in "Proc. 1st Int. Conf. Carbon," Berlin, 2000, p. 1035.
52. X. Chen, Y. Hishikawa, and S. Motojima, in "Proc. 1st Int. Conf. Carbon," Berlin, 2000, p. 1055.
53. K. Shibagaki, S. Motojima, and M. Hashimoto, *Mater. Technol.* 18, 400 (2001).
54. K. Shibagaki and S. Motojima, *Mater. Technol.* 19, 38 (2001).
55. K. Shibagaki, S. Motojima Y. Umemoto, and Y. Nishitani, *Carbon* 39, 1337 (2001).
56. S. Motojima and H. Iwanaga, *Mater. Technol.* 18, 12 (2000).
57. S. Motojima, Y. Itoh, S. Asakura, and H. Iwanaga, *J. Mater. Sci.* 30, 5049 (1995).
58. C. Kuzuya, Y. Hishikawa, S. Hirako, M. Fujii, H. Iwanaga, and S. Motojima, *Adv. Mater. CVD* 8, 57 (2002).
59. Y. Hishikawa, C. Kuzuya, S. Hirako, W.-I. Hwang, and S. Motojima, *Trans. Mater. Res. Soc. Jpn.* 27, 39 (2002).
60. S. Motojima, M. Kawaguchi, and H. Iwanaga, *TANSO* 151, 41 (1992).
61. S. Motojima, I. Hasegawa, S. Kagiya, S. Asakura, M. Kawaguchi, and H. Iwanaga, *J. Phys. IV* C3, 599 (1993).
62. S. Motojima, I. Hasegawa, S. Kagiya, M. Momiyama, M. Kawaguchi, and H. Iwanaga, *Appl. Phys. Lett.* 62, 2322 (1993).
63. S. Motojima, S. Asakura, M. Hirata, and H. Iwanaga, *Mater. Sci. Eng. B* 34, L9 (1995).
64. S. Motojima, S. Kagiya, and H. Iwanaga, *Mater. Sci. Eng. B* 34, 47 (1995).
65. S. Motojima, Y. Itoh, S. Asakura, and H. Iwanaga, *J. Mater. Sci.* 30, 5049 (1995).
66. S. Motojima, I. Hasegawa, S. Kagiya, K. Ando, and H. Iwanaga, *Carbon* 33, 1167 (1995).
67. S. Motojima, S. Asakura, S. Takeuchi, and H. Iwanaga, *Carbon* 34, 289 (1996).
68. S. Motojima, T. Hamamoto, and H. Iwanaga, *J. Cryst. Growth* 158, 79 (1996).
69. W.-In Hwang, X. Chen, T. Kuzuya, K. Kawabe, and S. Motojima, *Carbon* 38, 565 (2000).
70. W. In-Hwang, H. Yanagida, and S. Motojima, *Mater. Lett.* 43, 11 (2000).
71. X. Chen, S. Motojima, W. In-Hwang, M. Kohda, Y. Hishikawa, and H. Iwanaga, *Trans. Mater. Res. Soc. Jpn.* 25, 565 (2000).
72. X. Chen, W.-I. Hwang, and S. Motojima, *Mater. Technol.* 18, 229 (2000).
73. W.-In Hwang, X. Chen, and S. Motojima, *Mater. Technol.* 18, 263 (2000).
74. Y. Okada and K. Takeuchi, *J. Mater. Sci. Lett.* 11, 1715 (1992).
75. H. Takikawa, M. Yatsuki, R. Miyano, M. Nagayama, T. Sakakibara, et al., *Jpn. J. Appl. Phys.* 39, 5177 (2000).
76. C. Kuzuya, Y. Hayashi, and S. Motojima, *Carbon* 40, 1071 (2002).
77. S. Motojima, C. Kuzuya, Y. Hishikawa, and S. Shimada, *Trans. Mater. Res. Soc. Jpn.* 27, 109 (2002).
78. W. In-Hwang, K. Kawabe, and S. Motojima, *Mater. Sci. Eng. B* 86, 1 (2001).
79. C. Kuzuya, S. Motojima, M. Kohda, and Y. Hishikawa, *Mater. Technol.* 20, 3 (2002).
80. C. Kuzuya, M. Kohda, Y. Hishikawa, and S. Motojima, *Carbon* 40, 1991 (2002).
81. R. T. K. Baker and J. J. Chludzinski Jr., *J. Catal.* 64, 464 (1980).
82. X. Chen, W. In-Hwang, S. Shimada, M. Fujii, H. Iwanaga, and S. Motojima, *J. Mater. Res.* 15, 808 (2000).
83. X. Chen, S. Motojima, and H. Iwanaga, *Carbon* 37, 1825 (1999).
84. W. In-Hwang, T. Kuzuya, H. Iwanaga, and S. Motojima, *J. Mater. Sci.* 36, 971 (2001).
85. T. Hashishin, H. Iwanaga, and S. Motojima, *Mater. Technol.* 19, 293 (2002).
86. W. B. Downs and R. T. K. Baker, *Carbon* 29, 1173 (1991).
87. R. T. K. Baker, *Carbon* 27, 315(1989).
88. A. Fonseca, K. Hernadi, J. B. Nagy, Ph. Lambin, and A. A. Lucas, *Carbon* 33, 1759 (1995).
89. A. Fonseca, K. Hernadi, J. B. Nagy, P. H. Lambin, and A. A. Lucas, *Synthetic Metals* 77, 235 (1996).
90. D. Bernaerts, X. B. Zhang, X. F. Zhang, G. Van Tendeloo, S. Amelinckx, J. van Landuyt, V. Ivanov, and J. B. Nagy, *Philos. Mag.* 71, 605 (1995).
91. X. B. Zhang, X. F. Zhang, D. Bernaeets, G. Van Tendeloo, S. Amilinckx, J. Van Landuyt, V. Ivanov, J. B. Nagy, Ph. Lambin, and A. A. Lucas, *Europhys. Lett.* 27, 141 (1994).
92. J. H. Weaver, *Science* 265, 511 (1994).
93. Ph. Lambin, A. Fonseca, J.-P. Vigneron, J. B. Nagy, and A. A. Lucas, *Chem. Phys. Lett.* 245, 85 (1995).
94. B. L. Dunlap, *Phys. Rev. B* 46, 1933 (1992).
95. B. L. Dunlap, *Phys. Rev. B* 49, 5643 (1992).
96. B. L. Dunlap, *Phys. Rev. B* 50, 8134 (1992).
97. S. Ihara and S. Itoh, *Carbon* 33, 931 (1995).
98. W. Li, S. Xie, W. Liu, R. Zhao, Y. Zhang, W. Zhou, G. Wang, and L. Qian, *J. Mater. Sci.* 34, 2745 (1999).
99. X. Chen, T. Saito, M. Kusunoki, and S. Motojima, *J. Mater. Res.* 14, 4329 (1999).

100. X. Chen, S. Yang, and S. Motojima, *Mater. Lett.* 3751, 48 (2002).
101. R. T. Yang and J. P. Chen, *J. Catal.* 115, 52 (1989).
102. M. Liu and J. M. Cowley, *Carbon* 32, 393 (1994).
103. K. Akagi, R. Tamura, and M. Tsukada, *Phys. Lev. Lett.* 74, 2307 (1995).
104. S. Motojima, H. Asano, and H. Iwanaga, *J. Euro. Ceram. Soc.* 16, 989 (1996).
105. S. Motojima, S. Ueno, T. Hattori, and H. Iwanaga, *J. Cryst. Growth* 96, 383 (1989).
106. S. Motojima, Y. Kojima, T. Hamamoto, N. Ueshima, and H. Iwanaga, *Electrochem. Soc. Proc.* 97-39, 595 (1997).
107. X. Chen, Y. Hishikawa, W.-I. Hwang, T. Kuzuya and S. Motojima, *Electrochem. Soc. Proc.* 13, 385 (2000).
108. X. Chen, S. Motojima, and H. Iwanaga, *J. Cryst. Growth* 237–239, 1931 (2002).
109. S. Motojima, S. Yang, X. Chen, and H. Iwanaga, *J. Mater. Sci.* 34, 5989 (1999).
110. S. Motojima, W.-I. Hwang, X. Chen, and H. Iwanaga, *J. Electrochem. Soc.* 147, 1228 (2000).
111. S. Motojima, W.-I. Hwang, and X. Chen, *Mater. Res. Bull.* 35, 1517 (2000).
112. S. Motojima, W.-I. Hwang, and H. Iwanaga, *J. Mater. Sci.* 36, 673 (2001).
113. K. Kaneto, M. Makoto, and S. Motojima, *T. IEE Japan* 118, 1425 (1998).
114. K. Kaneto, M. Tsuruta, and S. Motojima, *Synthetic Metals* 103, 2578 (1999).
115. M. Fujii, M. Matsui, S. Motojima, and Y. Hishikawa, *Thin Solid Films* 409, 78 (2002).
116. M. Fujii, S. Matui, S. Motojima, and Y. Hishikawa, *J. Cryst. Growth* 237–239, 1937.
117. L. Pan, T. Hayashida, M. Zhang, and Y. Nakayama, *Jpn. J. Appl. Phys.* 40, 235 (2001).
118. S. Motojima and H. Iwanaga, *Kinou Zairyou* 17, 1 (1997).
119. V. K. Varadan, private communication.
120. S. Motojima, H. Iwanaga, and V. K. Varadan, *Hyomen* 36, 140 (1998); *EMC* 120, 50 (1998).
121. J.-H. Du, C. Sun, S. Bai, G. Su, Z. Ying, and H.-M. Cheng, *J. Mater. Res.* 17, 1232 (2002).
122. S. Motojima, W. In-Hwang, T. Kuzuya, and H. Iwanaga, *J. Mater. Sci.* 36, 71 (2001).
123. K. Shibagaki and S. Motojima, *Carbon* 39, 411 (2001).
124. S. Motojima, S. Ueno, T. Hattori, and H. Iwanaga, *J. Cryst. Growth* 96, 383 (1989).
125. S. Motojima, M. Kawaguchi, K. Nozaki, and H. Iwanaga, in "Proc. 11th Int. Conf. on CVD," Seattle, 1990, p. 573.
126. A. Addamiano, *J. Cryst. Growth* 58, 617 (1982).
127. T.-K. Kang, S.-D. Park, C.-K. Rhee, and I1-H. Kuk, in "Proc. 5th Japan–Korea Ceramic Seminar," Kobe, 1989, p. 249.
128. S. Motojima, S. Kagiya, and H. Iwanaga, *J. Mater. Sci.* 31, 4641 (1996).
129. S. Motojima, I. Hasegawa, and H. Iwanaga, *J. Phys. IV* C5, 1061 (1995).
130. H. Iwanaga, S. Motojima, M. Ichihara, and S. Takeuchi, *J. Cryst. Growth* 100, 271 (1990).
131. H. Iwanaga, T. Iwasaki, S. Motojima, and S. Takeuchi, *J. Mater. Lett.* 9, 731 (1990).
132. H. Iwanaga, T. Iwasaki, and S. Motojima, *J. Sur. Finishing Soc. Jpn.* 41, 578 (1990).
133. S. Motojima, T. Yamana, T. Araki, and H. Iwanaga, *J. Electrochem. Soc.* 142, 3141 (1995).
134. H. Iwanaga, M. Kawaguchi, and S. Motojijma, *Jpn. J. Appl. Phys.* 32, 103 (1993).
135. U. Vogt, H. Hoffmann, and V. Kramer, *Key Eng. Mater.* 89, 29 (1994).
136. S. Motojima, S. Kagiya, and H. Iwanaga, *Mater. Sci. Eng. B* 34, 159 (1995).
137. S. Motojima, I. Hasegawa, M. Kawaguchi, K. Nozaki, and H. Iwanaga, *J. Chem. Vapor deposition* 1, 137 (1992).
138. S. Motojima, T. Kuzuya, W.-I. Hwang, X. Chen, M. Fujii, and H. Iwanaga, *J. Phys. IV France* 9, 8 (1999).
139. S. Yang, N. Ueshima, and S. Motojima, *Mater. Sci. Eng. A* 346, 29 (2003).
140. K. Robbie and M. J. Brett, *J. Vac. Sci. Technol. A* 15, 1460 (1997).
141. J. C. Sit, D. J. Borer, and M. J. Brett, *Adv. Mater.* 12, 371 (2000).
142. K. Robbie, D. J. Broer, and M. J. Brett, *Nature* 399, 764 (1999).
143. J. Ballato, R. E. Riman, J. R. Vig, and S. M. Laffey, *J. Mater. Res.* 13, 3144 (1998).
144. S. M. Yang, I. Sokolov, N. Coombs, C. T. Kresge and G. A. Ozin, *Adv. Mater.* 11, 1427 (1999).
145. K. Sugiyasu, S. Tamaru, M. Takeuchi, D. Berthier, I. Huc, R. Oda, S. Shinkai, *Chem. Commun.* 2002, 1212 (2002).
146. S. Motojima et al., in preparation.
147. P. Gleize, M. C. Schouler, P. Gadelle, and M. Caillet, *J. Mater. Sci.* 29, 1597 (1994).
148. S. Johansson, J.-A. Schweitz, H. Westberg, and M. Boman, *J. Appl. Phys.* 72, 5956 (2002).
149. G. Jiang, H. Zhuang , J. Zhang, M. Ruan, W. Li, F. Wu, and B. Zhang *J. Mater. Sci.* 35, 57 (2000).
150. E. Schonherr and E. Winckler, *J. Cryst. Growth* 32, 117 (1976).
151. A. Addamiano, *Nature* 179, 493 (1957).
152. A. Addamiano, *J. Cryst. Growth* 11, 351 (1971).
153. K. Barner and H. Berg, *J. Cryst. Growth* 46, 763 (1979).
154. K. Kishi, *J. Cryst. Growth* 45, 517 (1978).
155. J. M. Garcia-Ruiz and J. L. Amoros, *J. Cryst. Growth* 55, 379 (1981).
156. J. M. Garcia-Ruiz, *J. Cryst. Growth* 73, 251 (1985).
157. S. Mann, *J. Chem. Soc., Dalton Trans.* 21, 3953 (1997).
158. J. D. Hopwood and S. Mann, *Chem. Mater.* 9, 1819 (1997).
159. L. A. Gower and D. A. Tirrell, *J. Cryst. Growth* 191, 153 (1998).
160. Q. Huo, D. Zhao, J. Feng, K. Weston, S. K. Buratto, G. D. Stucky, S. Schacht, and F. Schuth, *Adv. Mater.* 9, 974 (1997).
161. C. D. C. E. Lakeman, G. Pan, N. Muto, M. Miyayama, H. Yanagida, and D. A. Payne, *Mater. Lett.* 13, 330 (1992).
162. S. Motojima, S. Yang, X. Chen, and H. Iwanaga, *Mater. Res. Bull.* 35, 203 (2000).